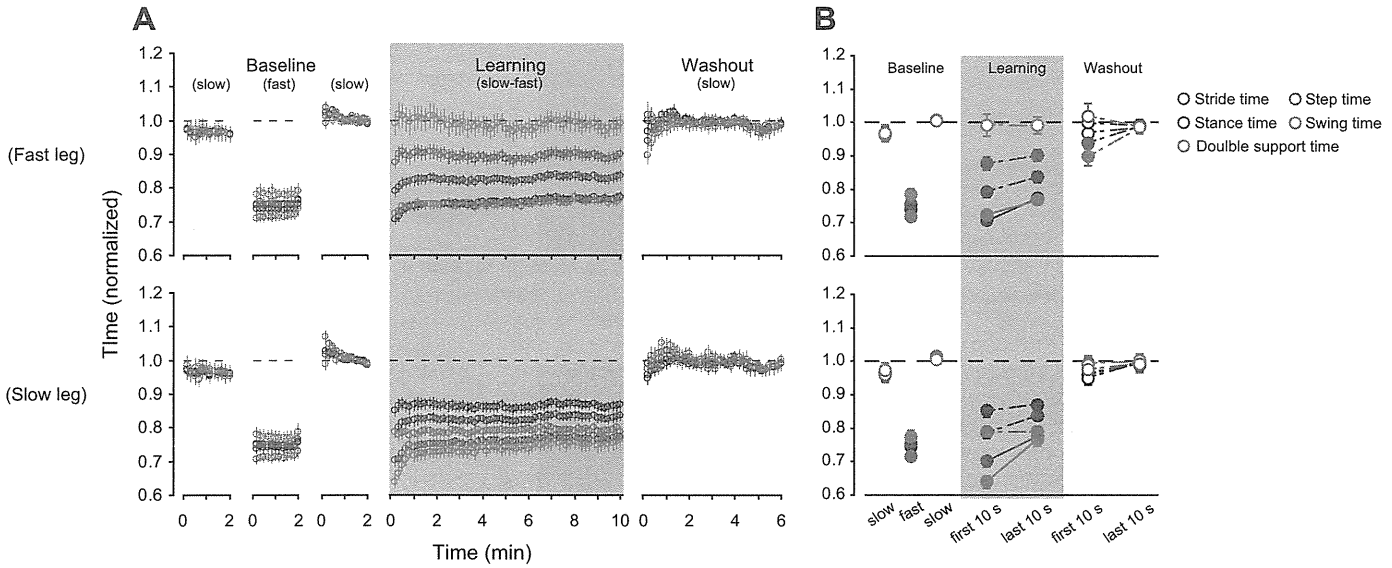

Fig. 2. *A*: mean of the time series changes of the temporal parameters for the whole experimental protocol (fast leg on the *top row* and slow leg on the *bottom row*). *B*: comparisons of each parameter at different time points. All the data were normalized to those of the baseline (for details, see METHODS). Filled circles indicate statistically significant differences from those during the baseline period, and the solid lines show the significant differences between the variables. Error bars indicate means ± SE. Differences were considered statistically significant when $P < 0.05$.

differences the changes could be categorized into three different patterns. The results are described in Fig. 3 for the whole experimental protocol (*left*) and for the comparison among different time points (*right*) to address the capability of adaptation. Figure 3, *middle*, highlights the first part of each learning and washout periods. At the beginning of the adaptation period, the mediolateral and the posterior components (*A* and *D*) of GRF showed significant deviations from the baseline at the beginning of split-belt period in both the slow ($P < 0.05$ for mediolateral, and $P < 0.01$ for posterior) and the fast leg ($P < 0.001$ for mediolateral, and $P < 0.001$ for posterior). Here, the slow leg values were adjusted to be near those in the slow baseline and the fast leg values were adjusted to be near those in the fast baseline. In the adaptation period, the mediolateral component in the fast leg gradually decreased toward the fast baseline values after initial overshoot. The comparison between the first and last 10 s of the adaptation period showed a significant difference ($P < 0.05$). The other comparisons did not show such a change. Upon return to the tied belt condition, there were significant aftereffects in the fast ($P < 0.01$) and slow ($P < 0.01$) legs in the mediolateral component and only in the slow leg in the posterior component ($P < 0.05$). The vertical component, on the other hand (Fig. 3*B*), showed somewhat different behavior from the mediolateral or the posterior components described above. At the beginning of the adaptation period, the relationship between the values for the fast leg and those for the slow leg were flipped from the baseline values (the fast leg values approached the slow baseline values and the slow leg values approached the fast baseline values). Only the slow leg showed significant deviation from the baseline initially ($P < 0.01$), and it did not exhibit any capability of adaptation during the 10-min test period. There were no evident aftereffects in either the fast or slow legs in this component.

Among the four different components of the GRF, the anterior component showed the clearest signs of adaptation and washout in both legs (Fig. 3*C*). At the initial stage of the adaptation period, the mean value in the fast leg was adjusted to be close to the slow baseline value, whereas in the slow leg ($P < 0.001$) it was near the value of the fast baseline period. There were steep changes in the first min followed by moderate changes lasting for the remaining 9 min during the adaptation period, where the relationship between the legs flipped early in the period. At the completion of the adaptation period, the value in the fast leg was adjusted to be close to that of the fast baseline and the value in the slow leg was adjusted to be close to that of the slow baseline. There were significant differences between the first and last 10 s in both the fast ($P < 0.001$) and slow ($P < 0.001$) legs. The washout phase started with pronounced deviation from the baseline in both legs, and there were gradual changes toward the baseline values, with the overall pattern of change into the opposite direction to that during the adaptation period. The statistical comparisons demonstrated significant deviation from the baseline at the beginning of the washout phase [$P < 0.001$ (fast) and $P < 0.01$ (slow)] and differences between the initial and the last 10 s in the washout in both the fast ($P < 0.001$) and slow ($P < 0.01$) legs.

EMG responses. Figure 4 shows the time series changes in the EMG activity for the whole experimental protocol (*left*) and for the comparison among different time points at selected time periods during the stance and the swing phases (*right*). Generally, the EMG responses were more variable than were the temporal parameters and ground reaction force data.

During the initial stage of the adaptation period, activities in the BF muscle in the fast leg and the RF and TA muscles in the slow leg increased during the stance phase. The activity of these muscles exhibited a clear adaptive curve, with the values gradually decreasing toward the baseline values. At 10 min, the values were almost identical to the baseline values, despite the fact that the subject was walking on a split treadmill surface. The statistical comparison revealed in those muscles that there were initially significant differences from the baseline values [$P < 0.001$ (fast BF), $P < 0.001$ (slow RF), and $P < 0.01$

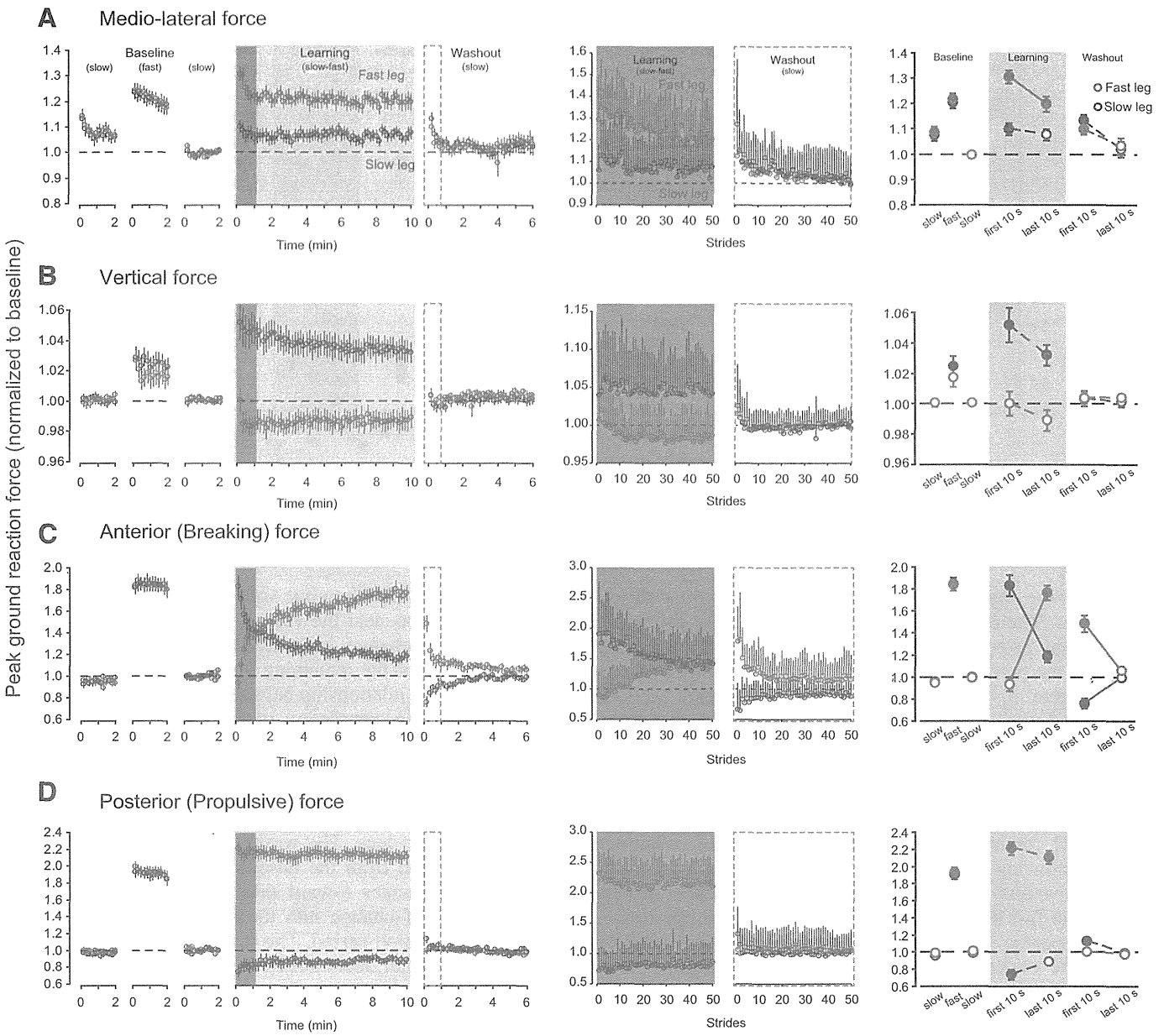

Fig. 3. Time series changes of the GRF components (*A*: lateral; *B*: vertical; *C*: anterior; *D*: posterior). Blue circles are the values for the slow leg under the "adaptation" period, and the red circles indicate those of the fast leg. Averaged value of each 10-s bin are shown at *left*, and each step data at the beginning of adaptation and washout periods (first 50 steps) are shown at *middle*. *Right*: comparisons of each parameter at different time points. All the data were normalized to those of the baseline values (for details, see METHODS). Filled circles indicate statistically significant differences from those during the baseline period, and the solid lines show the significant differences between the variables. Error bars indicate means ± SE. Differences were considered statistically significant when $P < 0.05$.

(slow TA)]. There were also statistically significant differences in these muscles between the initial and final 10 s in the 10-min adaptation phase, demonstrating the capability of adaptation [$P < 0.001$ (fast BF), $P < 0.001$ (slow RF), and $P < 0.01$ (slow TA)]. With the return to the tied belt condition, the TA, RF, and BF muscles in the fast leg and the MG and RF muscles in the slow leg showed augmented activity. Although the belt condition was identical to that in the baseline period, the EMG activities were significantly different from those in the baseline period [$P < 0.05$ (fast TA), $P < 0.01$ (fast RF), $P < 0.01$ (fast BF), $P < 0.01$ (slow MG), and $P < 0.05$ (slow RF)]. These activities gradually decreased toward the baseline level within the first 2 min or so. Around 5 min in the washout phase, the levels of these activities were similar to the baseline values.

During the swing phase, the TA ($P < 0.01$) and BF ($P < 0.01$) muscles in the fast leg and RF muscle in the slow leg ($P < 0.05$) showed augmented activities in the early adaptation period compared with those at baseline, where only the BF in the fast leg ($P < 0.05$) and the RF in the slow leg ($P < 0.05$) exhibited a clear pattern of adaptation. In the following washout period, only the BF muscle showed an initial enhancement of the activity ($P < 0.01$) and a pattern of washout ($P < 0.001$) toward the baseline level. In the RF muscles of the fast limb, the activities were lessened even below baseline levels ~5 min

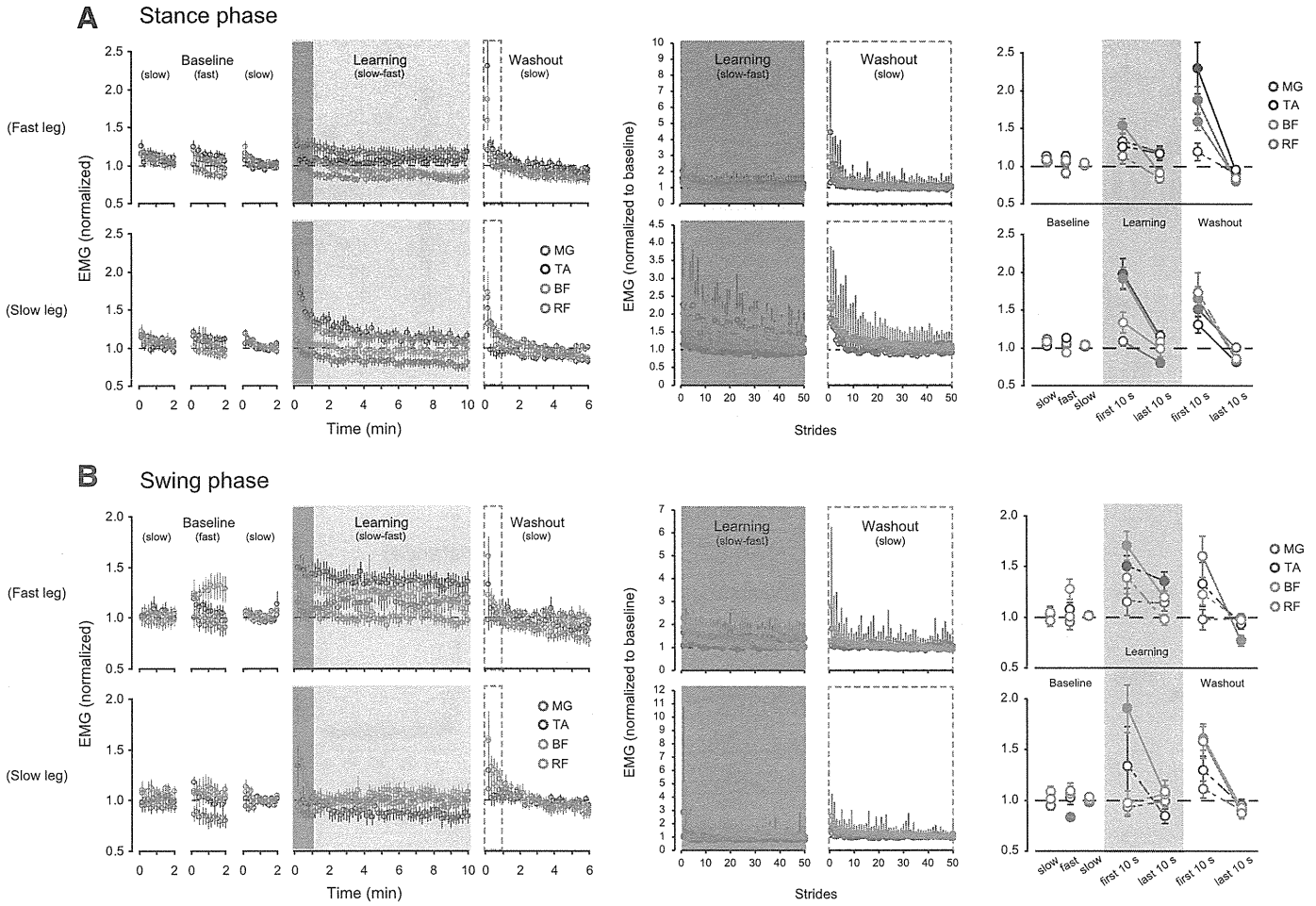

Fig. 4. *A* and *C*: mean of the time series changes of the EMG activities in each muscle investigated during the stance phase (*A*) and the swing phase (*C*). All the data were normalized to those under the baseline condition. *Top rows*: activities of the fast leg during the adaptation period, and the data in the lower rows are those of the slow leg. *B* and *D*: comparisons of the mean values at different time points. Filled circles indicate statistically significant differences from those during the baseline period, and the solid lines show the significant differences between the variable. Error bars indicate means ± SE. Differences were considered statistically significant when $P < 0.05$.

in the washout period ($P < 0.01$), and the reductions resulted in statistically significant differences between the initial and final 10 s of the period in both legs [$P < 0.01$ (fast) and $P < 0.01$ (slow)].

In contrast to the TA muscles during the stance phase (initially increased activity and subsequent decrement in the slow leg during the adaptation period and the emergence of the aftereffect in the fast leg), the activities in the MG exhibited contrastive behavior. Figure 5*A* presents representative EMG waveforms in the TA and MG muscles under stride cycles at different time points of the experiment. Figure 5*B* highlights a distinct adaptive process between the slow (blue) and fast (red) legs of the TA EMG in the early stance phase and the MG EMG in the late stance phase. At the initial stage of the adaptation period, the TA EMG in the slow leg showed higher values, and then at the completion of the adaptation period, the values in the fast leg were adjusted to be close to those of the fast baseline and the values in the slow leg were adjusted to be close to those of the slow baseline.

The washout phase started with a pronounced deviation from the baseline in the fast leg, and there were gradual changes toward the baseline values. In contrast to the TA muscle, only the slow leg showed significant deviation from the baseline initially ($P < 0.01$), and it did not exhibit any capability of adaptation during the 10-min test period in the MG muscle. In the washout period, both legs showed higher values and then gradually recovered to the baseline values. Figure 5*C* focuses on the EMG activity under particular phases and in particular muscles where activity is essential for functional gait, that is, the mean EMG activity of the TA muscle during the early stance phase and that of the MG muscle during the late stance phase. A pattern of adaptation and subsequent aftereffects with relatively longer time course is found in the TA muscle ($P < 0.01$ to the baseline in the early adaptation period and $P < 0.01$ between early and late adaptation periods in the slow leg, and $P < 0.05$ to the baseline in the early washout period and $P < 0.05$ between early and late washout periods in the fast leg), while such activities are less evident in the MG muscle.

Figure 5*D* shows the relationship between the extent of adaptation of the slow/fast leg and the washout of contralateral leg in each TA/MG muscle, respectively (*top/bottom*). The regression line and the correlation coefficient value and its significance are indicated in the figure. A significant positive correlation was found in both muscles ($P < 0.05$), suggesting that the EMG patterns obtained on one side in the adaptation

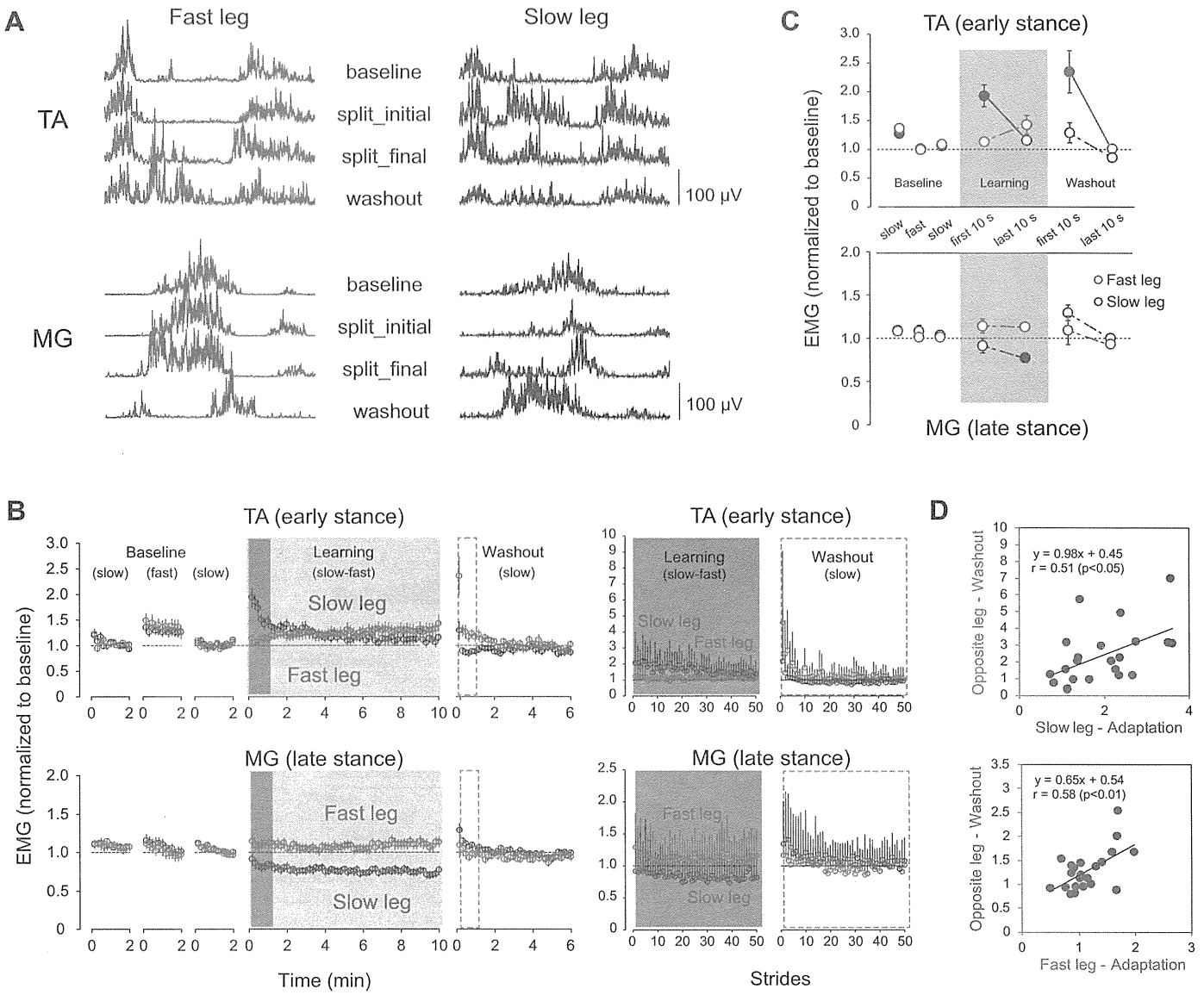

Fig. 5. *A*: representative waveforms of the EMG activities in the TA and MG muscles for both the fast and slow legs (those on the fast and slow belts during the adaptation period, respectively) at different time points. Each waveform represents an ensemble average of five consecutive stride cycles under the respective time points and is time normalized to stride cycles. *B*: mean of the time series changes of the EMG activities in the TA muscle during the first half of the stance phase and in the MG muscle during the last half of the stance phase. Filled circles represent the EMG activities during the first half of each gait cycle, and the open circles are those of the last half of the gait cycle. Averaged value of each 10 s bin are shown at *left*, and each step data at the beginning of adaptation and washout periods (first 50 steps) are shown at *right*. *C*: comparisons of each parameter at different time points (*top*: early stance of TA; *bottom*: late stance of MG). All the data were normalized to those of the baseline values (for details, see METHODS). Filled circles indicate statistically significant differences from those during the baseline period, and the solid lines show the significant differences between the variables. Error bars indicate means ± SE. Differences were considered significant at $P < 0.05$. *D*: relationship between the extent of adaptation of the slow/fast leg and the washout of the contralateral leg in the TA/MG muscle, respectively (*top/bottom*). Regression lines and the correlation coefficients and their significance are indicated in *A–D*.

period and the other side in the washout period switched with each other.

Relationship between the different variables. Figure 6 illustrates the relationship between the extent of adaptation and aftereffects for each variable (EMG_MG, EMG_TA, GRF_Braking, GRF_Propulsive). In the TA muscle, a positive correlation between adaptation and aftereffects was found in the fast leg (fast leg: $r = 0.429$, $P < 0.05$, slow leg: $r = 0.29$, n.s.). In the MG muscle, both the fast and slow legs showed a positive correlation between adaptation and aftereffects (fast leg: $r = 0.755$, $P < 0.05$, slow leg: $r = 0.446$, $P < 0.05$). Regarding the GRF data, a significant negative correlation was found only in the braking force of the slow leg (fast leg: $r = -0.180$, n.s., slow leg: $r = -0.459$, $P < 0.05$). No significant correlation was found in propulsive force in both legs (fast leg: $r = -0.064$, n.s., slow leg: $r = -0.159$, n.s.).

Tied-random (control) condition. Figure 7 shows the time series changes of the step time, braking GRF, and EMG activity in TA and MG muscles during the tied-random condition and the split-belt treadmill condition. The tied-random condition did not show any aftereffect in the postperturbation period, whereas the split-belt treadmill condition showed clear aftereffects in the washout period.

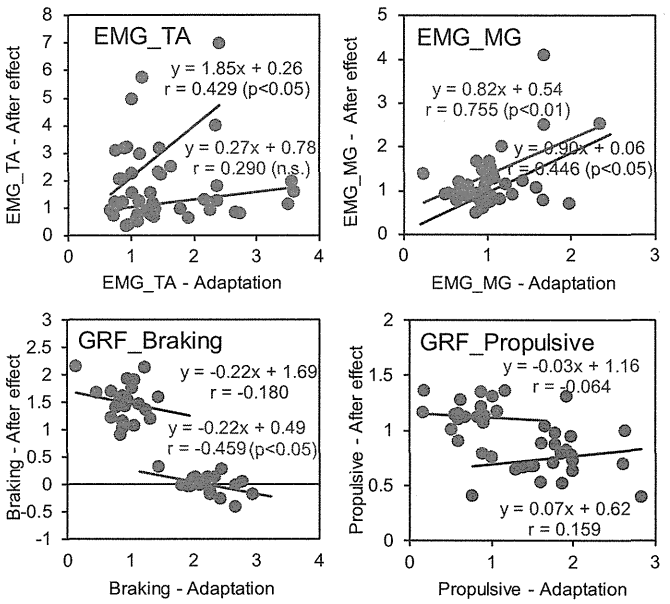

Fig. 6. Relationship between the extent of adaptation and washout for each variable (EMG_MG, EMG_TA, GRF_Braking, GRF_Propulsive). Regression lines and the correlation coefficients and their significance are indicated.

DISCUSSION

The purpose of this study was to elucidate the role of predictive and reactive feedback strategies during locomotor adaptations to split-belt treadmill walking. In the present study, we followed an experimental protocol used in Reisman et al. (2005), which was the first systematic study in a series of studies on split-belt treadmill adaptation. As clearly shown in the Fig. 3, the anterior component of the GRF showed a clear pattern of adaptation and subsequent aftereffects. Namely, the slow leg, through learning to walk on the slower belt, initially showed a significant increase in the braking force followed by a gradual decrease during the adaptation period, and then an abrupt reduction in the initial phase of washout. In contrast, the posterior component of GRF (propulsive force) showed a consistent increase/decrease in the fast/slow leg during the adaptation period and was not followed by subsequent aftereffects. The contrasting results between the braking and propulsive forces might reflect the existence of distinct control strategies underlying split-belt locomotor adaptation. The results obtained from lower limb EMG muscle also demonstrated a unique pattern due to the split-belt treadmill adaptation. In the following section, the detailed mechanisms underlying the split-belt treadmill adaptation and implications for the future use of the split-belt treadmill adaptation will be discussed.

Two distinct strategies underlying split-belt treadmill adaptation. The emergence of the adaptive and the subsequent de-adaptive phenomena with and after walking on a split-belt treadmill has been studied extensively by Bastian and colleagues over the last decade (Reisman et al. 2005, 2007, 2009; Morton and Bastian 2006; Choi et al. 2007, 2009; Vasudevan and Bastian 2010; Malone and Bastian 2010; Torres-Oviedo and Bastian 2010; Vasudevan et al. 2011; Musselman et al. 2011). Based on a series of split-belt treadmill experiments, Bastian and colleagues clearly dissociated different forms of locomotor adaptation, reactive and predictive adjustments, in the central nervous system. However, the details of the specific gait pattern adjustments made by subjects on an asymmetrically driven split-belt treadmill were not fully understood.

The novel contribution of the present study is to provide the specific patterns of the predictive feedforward and reactive feedback control strategies based on the GRF and EMG results. As clearly shown in the Fig. 3, the anterior component of the GRF in slow leg showed a clear pattern of adaptation and subsequent aftereffects, which is comparable to those originally identified in the reaching movement of the upper arm, which is the process for the recalibration of motor command with the new task demand (Kawato et al. 1987; Shadmehr and Mussa-Ivaldi 1994). Although the type of movement differs between upper limb motion and bipedal walking, adaptation to the split-belt treadmill can also be regarded as a process of trial-and-error-based adjustment of gait behavior in response to differently driven belts. At the initial part of split-belt walking, the central nervous system does not correctly predict the extent of perturbation and causal postural disturbance (movement error) due to the split belts. With continuous exposure to the split-belt condition, the subjects could finally establish the predictive feedforward motor command that enabled them to minimize the extent of postural disturbance presented by the split-belt condition.

Concerning this point, the authors of previous studies suggested the significance of feedforward mechanisms in human locomotion by comparing specific muscle activity during an "adapted state" in an imposed force field and upon the unexpected removal of the force field with the use of gait robotics (Lam et al. 2006) and an elastic band (Blanchette and Bouyer 2009). Taking the present results into account together with these previous findings, it is likely that the process comprising the braking force can be regarded as a predictive feedforward component of the motor control for bipedal walking. Given the importance of cerebellar function for acquiring the predictive feedforward model (Imamizu et al. 2000; Bastian 2006), similar neural processes might be involved in the split-belt treadmill adaptation.

In contrast, the posterior GRF showed a consistent increase/decrease in the fast/slow leg during the adaptation period and was not followed by subsequent aftereffects, suggesting that propulsive force can be regarded as the result of reactive adjustment which is presumably generated by an automatic feedback action. The manner of changes between anterior and posterior forces might reflect the existence of distinct control strategies underlying split-belt locomotor adaptation. We next discuss the possible mechanisms underlying GRF results based on our measurement of EMG activity.

Different role of each limb for accomplishing split-belt treadmill adaptation. In light of the asymmetrically driven support surface used in the present study, we suspect that the slow and fast legs have different functional roles for the accomplishment of gait adaptation. As indicated above, control of the braking force might involve an error-based learning process. Importantly, slower side plays a significant role as a "reference" for adaptation to walk normally under the novel circumstance of moving on an asymmetrically driven split-belt treadmill. Higher vertical GRF in the slow leg during the adaptation period also reflects that the subject tended to put much weight on this side.

As shown in Fig. 6, while the fast and slow legs show similar relationships between the extent of adaptation and the subse-

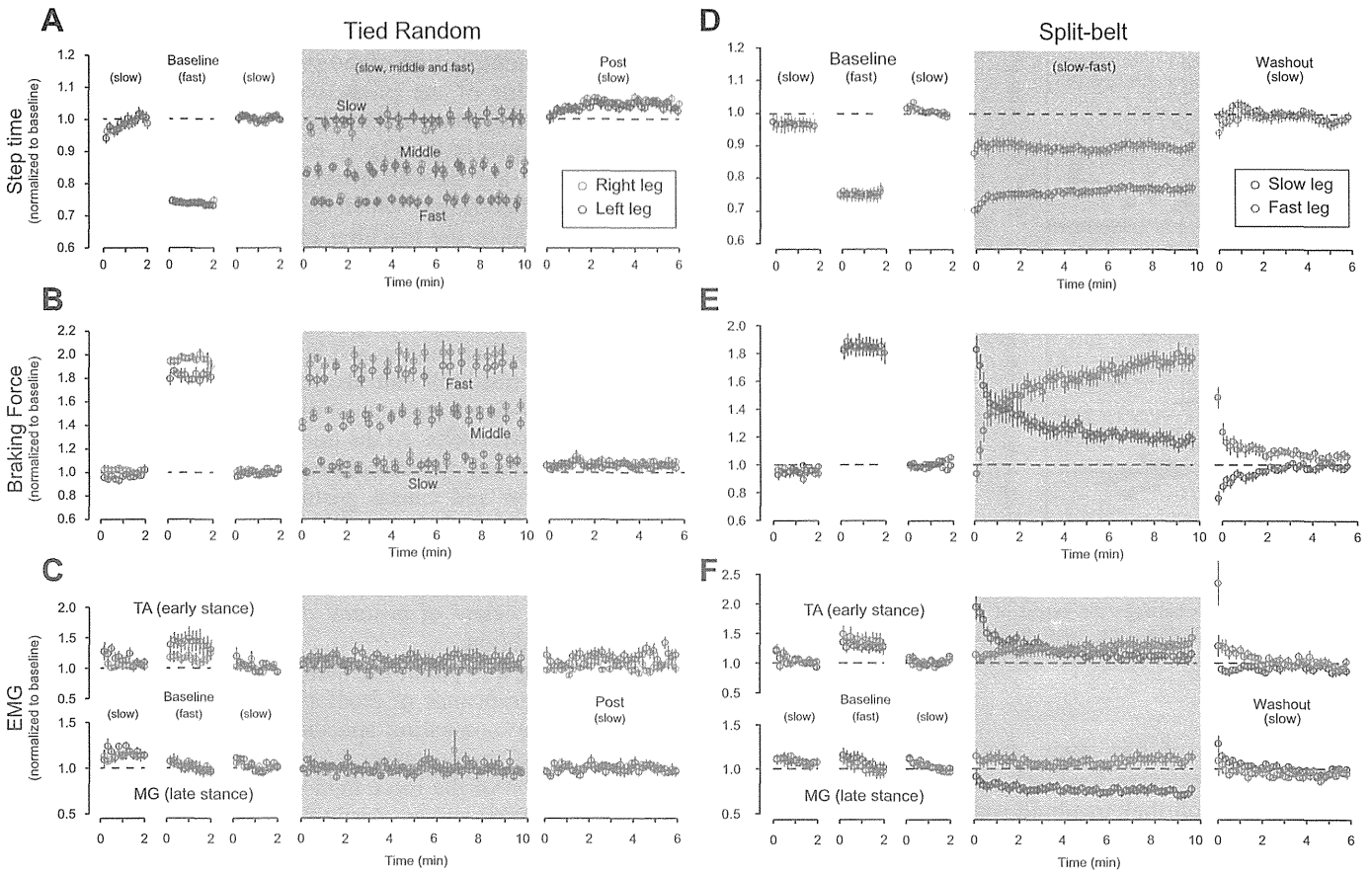

Fig. 7. Time series changes of the step time (*A* and *D*), braking GRF (*B* and *E*), and EMG activity in the TA and MG muscles (*C* and *F*) during the tied-random condition (*left*) and the split-belt treadmill condition (*right*). *Left*: cyan and magenta circles are the values for the right and left leg, respectively. *Right*: blue and red circles are the values for the slow and fast legs during the split-belt condition, respectively. Averaged values of each 10-s bin are shown. All data were normalized to those of the baseline values.

quent aftereffects in the EMG activity of the MG muscle, other parameters showed a clear difference between the slow (blue) and fast leg (red). These results also suggested different roles of each leg in split-belt adaptation. These interpretations are in agreement with the previous study stated that the slow moving leg was used as the primary support to stabilize the body equilibrium during the prolonged swing of the contralateral leg (Dietz et al. 1994; Duysens et al. 2004). Moreover, our results are in line with the previous report that the emergence of aftereffects after walking on an asymmetrically driven treadmill surface was always merged with a speed identical to that of the slower side during the adaptation periods (Vasudevan et al. 2010).

In addition to the contrasting braking force results between the fast and slow legs, other GRF parameters also showed remarkable differences between the legs, e.g., the larger shift of the lateral GRF and the enhancement of propulsive force in the fast leg. These results might reflect the larger amount of perturbation in the fast leg during the stance phase of walking. It is noteworthy that lateral GRF in the fast leg showed some extent of adaptation and subsequent aftereffect. The adaptive changes observed in the lateral and braking forces suggest that the maintenance of balance would be one of the necessary outcomes to achieve stable walking in the split-belt condition. Regarding this point, Finley et al. (2013) revealed that acquisition of an economical movement pattern is an important element of locomotor adaptation to novel environments. The reduction in metabolic power might be relevant to acquired stable walking as the result of split-belt treadmill adaptation.

Detail mechanisms underlying split-belt adaptation. As shown in Fig. 4, EMG responses in the TA, RF, and BF muscles during the stance phase and the BF muscle during the swing phase showed clear adaptive and de-adaptive processes. Most interestingly, the time series changes of the muscle activity in the TA muscles, especially during the early stance phase, resembled those of the braking force (Figs. 3 and 5). Duysens et al. (2004) also reported that the TA muscle remains active throughout most of the stance phase of the slow moving leg during split-belt treadmill walking. They interpreted this inadvertent activity as a result of coactivation of agonistic and antagonistic leg muscles to stabilize body equilibrium during the prolonged swing of the contralateral leg.

The TA muscle is typically activated from the beginning of the leg swing to the early stance phase. The abovementioned coactivation period at the early stance phase might be functionally essential to stabilize the ankle joint securely soon after a heel strike (Nakazawa et al. 2004). During split-belt treadmill walking, adjustment of the ankle stiffness in response to split-belt-induced perturbation is quite important. In addition, the subject might learn a causal relationship between the extent of perturbation and optimal ankle stiffness by an error-based learning process during the adaptation period, and they may

finally acquire predictive control of the ankle stiffness at the heel contact.

Regarding the control of ankle stiffness in the early stance phase during walking, it was demonstrated that a significantly large motor-evoked potential (Capaday et al. 1999) and long-latency stretch reflex (Christensen et al. 2000) are induced in the TA muscle at the early stance during walking. These findings strongly suggested that the enhancement of the excitability of TA corticospinal and stretch reflex pathways is necessary as an action to prepare for the upcoming perturbation at the heel contact. In light of these findings, it is likely that the total involvement of the cortical process is relatively larger at the beginning of adaptation to the split-belt-induced perturbation and, then, error-based learning enables the subject to update the internal model for walking, which presumably takes place in the cerebellum (Morton and Bastian 2006, Jayaram et al. 2012).

It might be speculated that the adaptation and subsequent aftereffects observed in split-belt treadmill walking are due merely to the difficulty of treadmill walking because some parameters showed gradual changes even during the baseline period. It is thus necessary to discuss the process of the induction of a learning effect due to split-belt treadmill walking. To investigate this matter, we conducted a supplemental experiment in 10 subjects with a protocol similar to that employed by Jayaram et al. (2011) using a protocol where the belts are tied the entire time but the speeds are frequently varied (every 10 s). Although the total duration and walking distance in this experimental condition were similar between the tied-random and split-belt treadmill walking, the tied-random condition did not show any aftereffect in the postperturbation period (Fig. 7).

This result suggests that the adjustment of gait behavior in response to bilateral belt speed changes does not require any updating process of the internal model for walking. During the tied-random condition, the subjects needed only a few steps to adjust their walking stability after the belt speed change. This is because humans can adjust their walking by using an automatically induced reflex system utilizing sensory feedback and previous experience. However, the split-belt treadmill-induced perturbation is unusual, and no prior experience can be used as a template for gait adjustment. As a result, the subjects achieved stable walking by their trial-and-error-based learning.

Conclusion and implication. The present results regarding GRF and muscle EMG activities provide useful information for discussions of the motor control and learning process during split-belt adaptation and subsequent aftereffects. Our findings indicate that predictive feedforward control is required to set optimal ankle stiffness in preparation for the impact at the heel contact, and passive feedback control is utilized for the production of reflexively induced propulsive force at the end of the stance phase during split-belt treadmill adaptation. This conclusion might have direct implications for the construction of specific rehabilitation protocols for the improvement of gait asymmetry in poststroke patients. It is plausible that interventions using a split-belt treadmill have the potential to make systematic adjustments of imbalances between breaking and propulsive forces and asymmetry between paretic and intact legs.

GRANTS

This work was supported by Grant-in-Aid for Young Scientists (A) (#22680045) to N. Kawashima and Grant-in-Aid for Young Scientists (B) to T. Ogawa (Research Project Number: 23700658) from Japan Society for the Promotion of Science.

DISCLOSURES

No conflicts of interest, financial or otherwise, are declared by the author(s).

AUTHOR CONTRIBUTIONS

Author contributions: T. Ogawa and N.K. performed experiments; T. Ogawa and N.K. analyzed data; T. Ogawa and N.K. interpreted results of experiments; T. Ogawa and N.K. prepared figures; T. Ogawa and N.K. drafted manuscript; N.K. conception and design of research; N.K. edited and revised manuscript; N.K., T. Ogata, and K.N. approved final version of manuscript.

REFERENCES

Bastian AJ. Learning to predict the future: the cerebellum adapts feedforward movement control. *Curr Opin Neurobiol* 16: 645–649, 2006.

Blanchette A, Bouyer LJ. Timing-specific transfer of adapted muscle activity after walking in an elastic force field. *J Neurophysiol* 102: 568–577, 2009.

Bowden MG, Balasubramanian CK, Neptune RR, Kautz SA. Anterior-posterior ground reaction forces as a measure of paretic leg contribution in hemiparetic walking. *Stroke* 37: 872–876, 2006.

Capaday C, Lavoie BA, Barbeau H, Schneider C, Bonnard M. Studies on the corticospinal control of human walking. I. Responses to focal transcranial magnetic stimulation of the motor cortex. *J Neurophysiol* 81: 129–139, 1999.

Choi JT, Bastian AJ. Adaptation reveals independent control networks for human walking. *Nat Neurosci* 10: 1055–1062, 2007.

Choi JT, Vining EP, Reisman DS, Bastian AJ. Walking flexibility after hemispherectomy: split-belt treadmill adaptation and feedback control. *Brain* 132: 722–33, 2009.

Christensen LO, Petersen N, Andersen JB, Sinkjaer T, Nielsen JB. Evidence for transcortical reflex pathways in the lower limb of man. *Prog Neurobiol* 62: 251–272, 2000.

Dietz V, Zijlstra W, Duysens J. Human neuronal interlimb coordination during split-belt locomotion. *Exp Brain Res* 101: 513–520, 1994.

Dietz V. Human neural control of automatic functional movement. *Physiol Rev* 71: 33–58, 1992.

Duysens J, Bastiaanse CM, Smits-Engelsman BC, Dietz V. Gait acts as a gate for reflexes from the foot. *Can J Physiol Pharmacol* 82: 715–722, 2004.

Finley JM, Bastian AJ, Gottschall JS. Learning to be economical: the energy cost of walking tracks motor adaptation. *J Physiol* 591: 1081–1095, 2013.

Jayaram G, Galea JM, Bastian AJ, Celnik P. Human locomotor adaptive learning is proportional to depression of cerebellar excitability. *Cereb Cortex* 21: 1901–1909, 2011.

Imamizu H, Miyauchi S, Tamada T, Sasaki Y, Takino R, Pütz B, Yoshioka T, Kawato M. Human cerebellar activity reflecting an acquired internal model of a new tool. *Nature* 403: 192–195, 2000.

Jayaram G, Tang B, Pallegadda R, Vasudevan EV, Celnik P, Bastian A. Modulating locomotor adaptation with cerebellar simulation. *J Neurophysiol* 107: 2950–2957, 2012.

Kawato M, Furukawa K, Suzuki R. A hierarchical neural-network model for control and learning of voluntary movement. *Biol Cybern* 57: 169–185, 1987.

Knutsson E. Gait control in hemiparesis. *Scand J Rehabil Med* 13: 101–108, 1981.

Lam T, Wolstenholme C, Yang JF. How do infants adapt to loading of the limb during the swing phase of stepping? *J Neurophysiol* 89: 1920–1928, 2003.

Lam T, Anderschitz M, Dietz V. Contribution of feedback and feedforward strategies to locomotor adaptations. *J Neurophysiol* 95: 766–773, 2006.

Malone LA, Bastian AJ. Thinking about walking: effects of conscious correction versus distraction on locomotor adaptation. *J Neurophysiol* 103: 1954–1962, 2010.

Morton SM, Bastian AJ. Cerebellar contributions to locomotor adaptations during splitbelt treadmill walking. *J Neurosci* 26: 9107–9116, 2006.

Musselman KE, Patrick SK, Vasudevan EV, Bastian AJ, Yang JF. Unique characteristics of motor adaptation during walking in young children. *J Neurophysiol* 105: 2195–2203, 2011.

Nakazawa K, Kawashima N, Akai M, Yano H. On the reflex co-activation of ankle flexor and extensor muscles induced by a sudden drop of support surface during walking in humans. *J Appl Physiol* 94: 604–611, 2004.

Prokop T, Berger W, Zijlstra W, Dietz V. Adaptational and learning processes during human split-belt locomotion: interaction between central mechanisms and afferent input. *Exp Brain Res* 106: 449–456, 1995.

Reisman DS, Block HJ, Bastian AJ. Interlimb coordination during locomotion: what can be adapted and stored? *J Neurophysiol* 94: 2403–2415, 2005.

Reisman DS, Wityk R, Silver K, Bastian AJ. Locomotor adaptation on a split-belt treadmill can improve walking symmetry poststroke. *Brain* 130: 1861–72, 2007.

Reisman DS, Wityk R, Silver K, Bastian AJ. Split-belt treadmill adaptation transfers to overground walking in persons poststroke. *Neurorehabil Neural Repair* 23: 735–744, 2009.

Reisman DS, McLean H, Bastian AJ. Split-belt treadmill training poststroke: a case study. *J Neurol Phys Ther* 34: 202–207, 2010.

Shadmehr R, Mussa-Ivaldi FA. Adaptive representation of dynamics during learning of a motor task. *J Neurosci* 14: 3208–3224, 1994.

Sinkjaer T, Andersen JB, Larsen B. Soleus stretch reflex modulation during gait in humans. *J Neurophysiol* 76: 1112–1120, 1996.

Torres-Oviedo G, Bastian AJ. Seeing is believing: effects of visual contextual cues on learning and transfer of locomotor adaptation. *J Neurosci* 30: 17015–17022, 2010.

Vasudevan EV, Bastian AJ. Split-belt treadmill adaptation shows different functional networks for fast and slow human walking. *J Neurophysiol* 103: 183–191, 2010.

Vasudevan EV, Torres-Oviedo G, Morton SM, Yang JF, Bastian AJ. Younger is not always better: development of locomotor adaptation from childhood to adulthood. *J Neurosci* 31: 3055–3065, 2011.

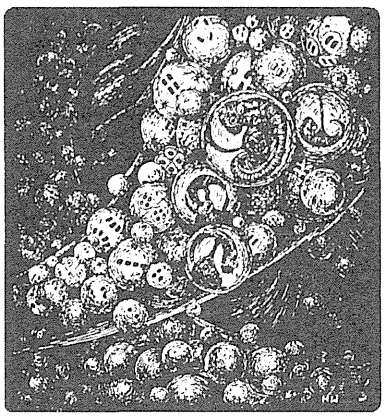

Zhang et al. Molecular Brain 2014, 7:14
http://www.molecularbrain.com/content/7/1/14

Molecular Brain

RESEARCH Open Access

Rewiring of regenerated axons by combining treadmill training with semaphorin3A inhibition

Liang Zhang[1,2,3†], Shinjiro Kaneko[1,4†], Kaoru Kikuchi[5], Akihiko Sano[5], Miho Maeda[5], Akiyoshi Kishino[5], Shinsuke Shibata[2], Masahiko Mukaino[3], Yoshiaki Toyama[1], Meigen Liu[3], Toru Kimura[5], Hideyuki Okano[2*†] and Masaya Nakamura[1*†]

Abstract

Background: Rats exhibit extremely limited motor function recovery after total transection of the spinal cord (SCT). We previously reported that SM-216289, a semaphorin3A inhibitor, enhanced axon regeneration and motor function recovery in SCT adult rats. However, these effects were limited because most regenerated axons likely do not connect to the right targets. Thus, rebuilding the appropriate connections for regenerated axons may enhance recovery. In this study, we combined semaphorin3A inhibitor treatment with extensive treadmill training to determine whether combined treatment would further enhance the "rewiring" of regenerated axons. In this study, which aimed for clinical applicability, we administered a newly developed, potent semaphorin3A inhibitor, SM-345431 (Vinaxanthone), using a novel drug delivery system that enables continuous drug delivery over the period of the experiment.

Results: Treatment with SM-345431 using this delivery system enhanced axon regeneration and produced significant, but limited, hindlimb motor function recovery. Although extensive treadmill training combined with SM-345431 administration did not further improve axon regeneration, hindlimb motor performance was restored, as evidenced by the significant improvement in the execution of plantar steps on a treadmill. In contrast, control SCT rats could not execute plantar steps at any point during the experimental period. Further analyses suggested that this strategy reinforced the wiring of central pattern generators in lumbar spinal circuits, which, in turn, led to enhanced motor function recovery (especially in extensor muscles).

Conclusions: This study highlights the importance of combining treatments that promote axon regeneration with specific and appropriate rehabilitations that promote rewiring for the treatment of spinal cord injury.

Keywords: Axonal regeneration, Semaphorin3A, Inhibitor, Rehabilitation, Rewiring, Drug delivery system

Background

Severe spinal cord injuries (SCI) in adult mammals result in various deficits throughout life. The limited capability of axons to regenerate in the central nervous system (CNS) is thought to be the main reason for these lasting deficits. Previous studies have suggested that both extrinsic and intrinsic factors in the CNS contribute to this incapacity for axonal regeneration [1-4]. Several distinct extrinsic molecules have been proposed to hinder axonal regeneration, including CNS myelin-associated proteins (MAG, Nogo, OMgp) [5-9], chondroitin sulphate proteoglycans [10,11], semaphorin3A [12,13] and RGM (repulsive guidance molecule) [14,15]. Neutralizing one (or several) of these molecules enhances axonal regeneration and results in some degree of functional recovery [10,16,17]. Until recently, it remained unknown whether neutralizing semaphorin3A would also lead to axonal regeneration and motor function recovery, in part because semaphorin3A deficiency is lethal [18]. Thus, we previously developed a selective and potent semaphorin3A inhibitor called SM-216289 [19] that selectively inhibits semaphorin3A signaling both *in vitro* and *in vivo* [20]. Administration of SM-216289 to adult rats after total spinal cord transection

* Correspondence: hidokano@a2.keio.jp; masa@a8.keio.jp
†Equal contributors
[2]Department of Physiology, Keio University School of Medicine, 35 Shinanomachi, Shinjuku, Tokyo 160-8582, Japan
[1]Department of Orthopedic Surgery, Keio University School of Medicine, 35 Shinanomachi, Shinjuku, Tokyo 160-8582, Japan
Full list of author information is available at the end of the article

(SCT) led to axonal regeneration and motor function recovery [20]. In addition, axonal regeneration and functional recovery have now been observed after several treatments that block 1 or more axonal growth inhibitors (including SM-216289). However, these effects are moderate at best, presumably because most of the regenerated axons do not connect with the correct targets [21]. Thus, rebuilding the appropriate connections of regenerated axons in lesioned spinal cords remains an important unresolved issue.

Body weight-supported treadmill training induces plastic changes in lesioned spinal cords and is useful for maximizing residual locomotor function after moderate SCI [22,23]. Furthermore, even after severe SCI, treadmill training partially improves hindlimb coordination [24] by inducing plasticity in specific spinal locomotor circuits called "central pattern generators" (CPGs). More specifically, these plastic changes have been shown to result in the recovery of plantar step walking in cats [25] and neonatal rats [26]. Furthermore, SCT adult rats partially recover plantar step walking when treadmill training is combined with other appropriate treatments, such as epidural electrical stimulation [27], pharmacological treatments [24] or cell transplantation [28]. Thus, with specific and appropriate rehabilitation, spinal cord CPGs can be reorganized, and functionally appropriate connections between CPGs and regenerated (or residual) axons can be rebuilt. Therefore, we hypothesized that extensive treadmill training would assist in the correct wiring of axons regenerated by semaphorin3A inhibitor treatment and that this rewiring may contribute to further motor functional recovery after SCT.

However, several issues, including drug delivery, remain to be resolved before semaphorin3A inhibitors can be used in the clinic. In an attempt to resolve these issues, we developed a novel selective semaphorin3A inhibitor, SM-345431 (Vinaxanthone), which demonstrates physicochemical properties equivalent to those of SM-216289 but also improvements that should allow for the development of a higher quality pharmaceutical product. Additionally, we developed a novel drug delivery system (DDS) utilizing a silicone sheet. With future clinical applications in mind, we chose to evaluate SM-345431 with this novel DDS. We observed that, consistent with our previous study [20], SM-345431 treatment enhanced axon regeneration and resulted in significant, but limited, hindlimb motor function recovery. Although extensive treadmill training with SM-345431 administration did not further improve axon regeneration, hindlimb motor performance was restored, as evidenced by the execution of plantar steps on a treadmill using a body support system (BSS). Moreover, immunohistological analysis suggested that SM-345431 administration with treadmill training reinforced the wiring of CPGs in lumbar spinal circuits and led to enhanced motor function recovery, especially in extensor muscles.

Results

Evaluation of a novel DDS and the activity of SM-345431 *in vitro*

In our previous study, we used an osmotic mini-pump to deliver the semaphorin3A inhibitor SM-216289 [20]. However, in clinical practice, this type of invasive drug delivery method is not ideal. Therefore, we developed a novel DDS that utilizes a silicone matrix to continuously deliver SM-345431 (a newly developed semaphorin3A inhibitor) intrathecally. We evaluated the drug release profile of SM-345431 in this new silicone matrix preparation and the potency of SM-345431-mediated semaphorin3A inhibition in vitro (Figure 1). SM-345431 exhibited semaphorin3A inhibiting activity with an IC50 of 0.1-0.2 μM in growth cone collapse assays using E8 chick and E14 rat dorsal root ganglia (DRG) (Figure 1A). When chick embryonic DRG explants and semaphorin3A-expressing COS7 cell aggregates (semaphorin3A-COS) were co-cultured in a collagen gel, the neurites of the DRG explants grew away from the semaphorin3A-COS, as shown in Figure 1B. However, when DRG explants and semaphorin3A-COS were co-cultured in the presence of SM-345431, radial extensions of the neurites were observed, which suggests that the chemo-repulsive effects of semaphorin3A were blocked by SM-345431 in a dose-dependent manner (Figure 1B). We also evaluated the selectivity of SM-345431 for semaphorin3A inhibition by examining the pharmacological profile of SM-345431 (Tables 1 and 2). As shown in these tables, the IC50 value for semaphorin3A inhibition was substantially lower than the other IC50s, which suggested that SM-345431 is a highly selective semaphorin3A inhibitor. To examine the semaphorin3A inhibiting activity of SM-345431 while it was being released from the silicone matrix (SM-345431-silicone), 1 mg of a silicone sheet containing 100 μg SM-345431 was placed into collagen gel cultures containing DRG explants and semaphorin3A-COS (Figure 1C). Assuming that 5% of the SM-345431 was released and uniformly diffused throughout the culture during the 2 days of incubation, the final concentration of SM-345431 was approximately 5 μM, which is a large enough dose to inhibit semaphorin3A activity. Radial neurite extension was observed in cultures with SM-345431-silicone but not in those with control silicone, indicating that semaphorin3A activity had been inhibited by SM-345431. We also measured the cumulative percentage of released doses of SM-345431 using this DDS over 2 months *in vitro* (Figure 1E) and found that this DDS released a constant dose of SM-345431 and was stable *in vitro*. When 7 mm × 5 mm × 0.3 mm sheets were used, the amount of drug release stabilized at approximately 10 μg/day after an initial peak of drug release that occurred over the first 2 days (Figure 1F). For the *in vivo* study, we trimmed the silicone sheet into 3 mm × 3 mm × 0.3 mm pieces to fit the injury site following SCT (Figure 1G-I).

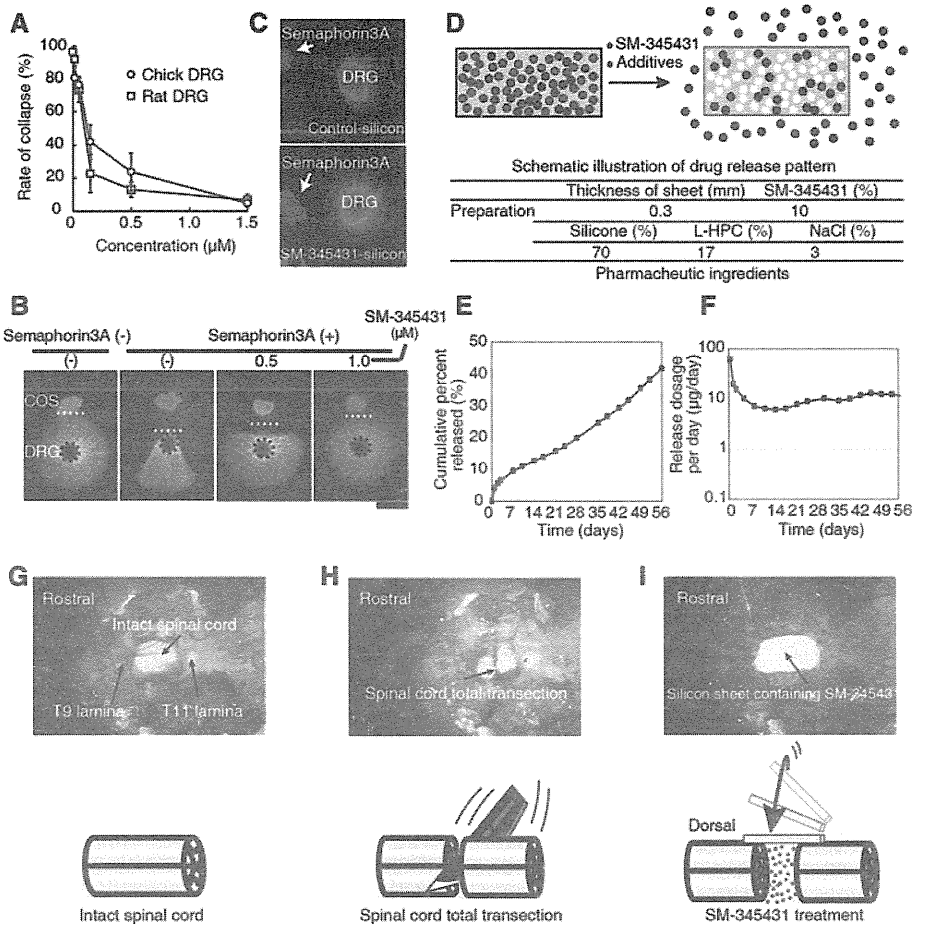

Figure 1 Preparation of the SM-345431 silicone DDS and *in vitro* release study. **(A)** Analysis of the inhibitory activity of SM-345431 in the growth cone collapse assay using E8 chick and E14 rat DRGs. **(B)** Collagen co-culture assay using E8 chick DRGs and semaphorin3A-expressing COS7 cell aggregates. **(C)** Pictures showing the effects of SM-345431-silicone or control-silicone in the collagen gel. **(D)** Schematic illustration of drug release from the matrix silicone preparation; the drug is dissolved in water, permeates into the preparation and is then released. The rate of water permeation into the silicone matrix is controlled by various additives, and the proportions of these additives included in the DDS control the variations in the drug release profile. The preparation used here contained the water-soluble additives listed in the table **(D)**. Stable and linear release of SM-345431 was observed for up to 2 months as shown in **(E)** and **(F)**. **(E, F)** SM-345431 release curve for the preparation. The linear cumulative percent release curve at 2 months **(E)** and the stable release dosage per day **(F)** are shown for the administration of SM-345431 using this novel DDS. **(G)** Exposed intact spinal cord. **(H)** Transected spinal cord. **(I)** The novel DDS we employed. A silicone sheet containing SM-345431 was placed onto the transected site of the spinal cord. The system allowed for stable and continuous release of the semaphorin3A inhibitor throughout the experimental period.

The release of SM-345431 (0.1 mg/mg loading 10%) *in vivo* was calculated as 0.5-0.7 μg/day, and this dose was similar to the dose of the semaphorin3A inhibitor (SM-216289) [19] that we administered using osmotic mini pumps in our previous study [20]. Therefore, the newly developed DDS allowed stable and continuous release of the newly developed, potent semaphorin3A inhibitor SM-345431.

SM-345431 delivery via the novel DDS enhanced axonal regeneration

To examine the regeneration of axons after SM-345431 treatment and SM-345431 treatment combined with extensive treadmill training, we evaluated axons in the injured spinal cord with immunostaining using antibodies against GAP43 and serotonin (5-HT) (Figure 2), GAP43 is widely used as a marker for regenerated axons. In both treatment groups, a marked increase in the number of GAP43-positive axons was observed at the epicenter of the injury (Figure 2D-F) and in the surrounding area (Figure 2G-I). Compared with the control group, the number of GAP43 axons was significantly increased in both the SM-345431 treatment group and the combined treatment group, especially at 1 mm caudal to the injury epicenter (Figure 2J). No significant difference was observed between the 2 treatment groups. Thus, administration of the semaphorin3A inhibitor SM-345431 using this DDS enhanced axonal

Table 1 Pharmacological profile of SM-345431 (part 1)

Enzymes	IC50 (μm)
Semaphorin	0.1-0.2
Matrix Metalloproteinase-1 (MMP-1)	>10
Matrix Metalloproteinase-7 (MMP-7)	10
Matrix Metalloproteinase-2 (MMP-2)	>10
Matrix Metalloproteinase-3 (MMP-3)	>10
Matrix Metalloproteinase-9 (MMP-9)	>10
Phospholipase PLA2-1	>10
Phospholipase PLC	>10
Caspase 1	>10
Caspase 3	>10
Caspase 6	>10
Caspase 7	>10
Caspase 8	>10
Protein Tyrosine Phosphatase, CD45	>10
Protein Tyrosine Phosphatase, PTP1B	>10
Protein Tyrosine Phosphatase, PTP1C	>10
Protein Tyrosine Phosphatase, T-Cell	>10
Sphingomyelinase, Neutral (N-SMase)	>10
Chemokine CCR1	>10
Chemokine CCR2B	>10
Chemokine CCR4	>10
Chemokine CCR5	>10
Chemokine CXCR2 (IL-8B)	>10
Glucocorticoid	>10
Interleukin IL-1	>10
Interleukin IL-2	>10
Interleukin IL-6	>10
Tumor Necrosis Factor (TNF), Non-selective	>10
Adhesion, fibronectin-mediated	>10
Adhesion, ICAM-1-Mediated	>10
Adhesion, VCAM-1-Mediated	>10
Cell proliferation, B-Cell+LPS	>10
Cell proliferation, T-Cell+Con A	>10
Mediator release, IL-1beta	>10
Mediator release, IFN-gamma	>10
Mediator release, IL-10	>10
Mediator release, IL-2	>10
Mediator release, IL-4	>10
Mediator release, IL-5	>10
Mediator release, IL-6	>10
Mediator release, TNF-alfa, PBML	>10
Transcription response, NF-AT	>10
Transcription response, NF-kB	>10

Summary of the IC50 values for binding assays of various receptors and ion channels, and IC50 values for the inhibition of various enzymes. The IC50 value for semaphorin3A inhibition was extremely low compared to that of the other factors.

Table 2 Pharmacological profile of SM-345431 (part 2)

Kinases	IC50 (μm)
CaMKII	>10
CDK5/p35	>10
cSRC	>10
EGFR	0.90
EphA2	>10
EphA4	0.80
EphB2	0.68
EphB4	>10
Fes	>10
FGFR1	>10
FGFR2	>10
FGFR3	0.77
FGFR4	0.64
Flt1	>10
Flt3	>10
Fyn	>10
GSK3α	2.46
GSK3β	>10
IGF-1R	>10
JAK3	>10
KDR	>10
MAPK2	>10
MEK1	>10
MEK4	>10
MKK6	>10
PAK2	>10
PAK4	>10
PKA	>10
PKBα	>10
PKBβ	>10
PKCγ	>10
ROCK-I	>10
ROCK-II	>10
ROCK-II	>10
SAPK2a	>10
TrkA	>10
TrkB	>10
PI 3-Kγ	>10

Summary of the IC50 values revealed by inhibition tests for various kinases. The data in Tables 1 and 2 suggest that SM-345431 was highly selective for semaphorin3A inhibition.

regeneration. However, no additional axonal regeneration was observed when SM-345431 treatment was combined with treadmill training.

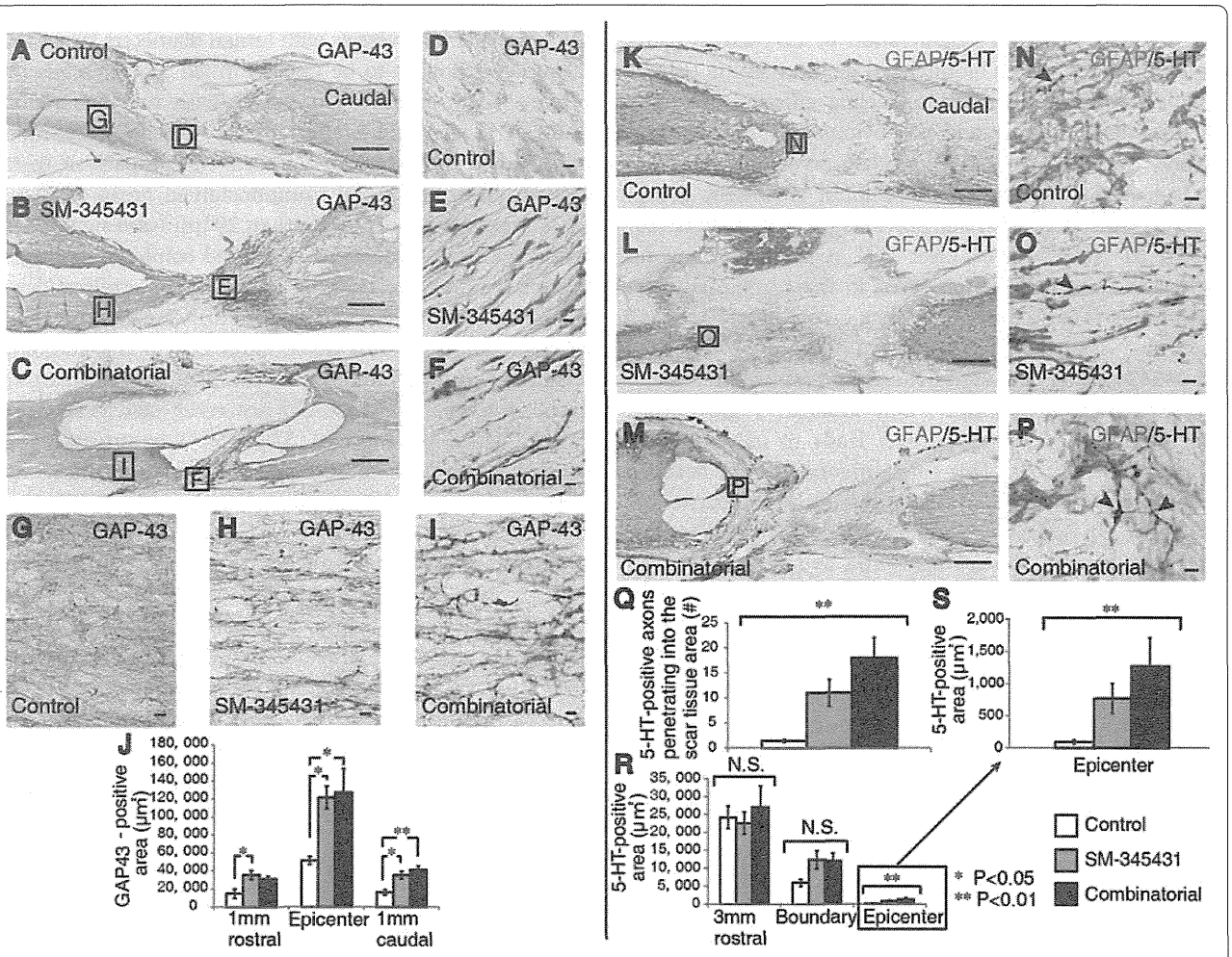

Figure 2 SM-345431 enhanced axonal regeneration *in vivo*, but combined treatment had only a limited effect on further axon regeneration. (A-I) Sagittal sections from SCT rats immunostained for GAP-43. Low-magnification images of the control **(A)**, SM-345431 **(B)** and combined treatment **(C)** groups. Scale bars = 500 μm. **(D-F)** Magnified images of the boxed areas shown in **A-C**. Scale bars = 10 μm. **(G-I)** Additional magnified images of the boxed areas shown in **A-C**. Scale bars = 10 μm. **(J)** Quantitative analysis of GAP-43-positive areas at 1 mm rostral to the lesion, 1 mm caudal to the lesion and at the epicenter of the lesion. Immunohistochemistry was performed using DAB with nickel enhancement. *P < 0.05, **P < 0.01. Statistical analyses were performed using one-way ANOVA and Bonferroni post hoc tests. Data are represented as the mean ± S.E.M. **(K-P)** Sagittal sections of SCT rats double-stained for 5-HT and GFAP. Scar tissue is outlined by GFAP staining, which also allowed for confirmation of total transection of the spinal cord in each animal. **(K-M)** Low-magnification images of the control **(K)**, SM-345431 **(L)** and combined treatment **(M)** groups. Scale bars = 500 μm. **(N-P)** Magnified images of the boxed areas shown in **K-M**. Scale bars = 10 μm. Arrowheads represent 5-HT-positive (serotonergic) axons. **(Q-S)** Quantitative analyses of 5-HT-positive axons that penetrated into the scar tissue. **(Q)** Quantitative analysis of the number of 5-HT-positive axons that penetrated into the lesion site. **(R,S)** Quantitative analysis of the 5-HT-positive area within the scar tissue area. Immunohistochemistry was performed by double-staining using DAB with or without nickel enhancement. The left side is rostral in all images. **P < 0.01. Statistical analyses were performed using a Kruskal-Wallis H test. Data represent the mean ± S.E.M.

The raphespinal tract axons, which can be detected by immunohistochemistry against serotonin (5-HT), contribute to functional locomotor control, and regeneration of these axons leads to substantial enhancement of motor function recovery [28]. Therefore, we also evaluated the regeneration of raphespinal tract axons using a GFAP antibody to delineate scar tissue at the injury site and a 5-HT antibody to visualize raphespinal axons. In control animals, 5-HT-positive axons were restricted to the area rostral to the transected site, and few 5HT-positive axons entered the GFAP-negative scar tissue area (Figure 2K,N). Interestingly, significantly more 5-HT-positive axons penetrated the GFAP-negative scar tissue area after SM-345431 treatment and combined treatment as compared to the control conditions (Figure 2K-S). Because we used a total transection model in this study, the 5-HT-positive axons that penetrated the GFAP-negative scar tissue in the treatment groups were regarded as regenerated axons (Figure 2L-P). Cortico-spinal tract (CST) axons are known to be incapable of regeneration after transection, even

following any of the previously reported treatments [7]. We next evaluated the regeneration of CST axons using the anterograde tracer biotinylated dextran amine (BDA). We first confirmed sufficient labeling efficiency of BDA tracing in each animal, and no obvious CST regeneration beyond the lesion epicenter was observed in either the control or the semaphorin3A inhibitor treatment group, which is consistent with our previous paper's findings [20] (Figure 3). Moreover, no clear CST regeneration beyond the lesion epicenter was observed in the combined treatment group (Figure 3).

SM-345431 enhanced angiogenesis and remyelination

Semaphorin3A suppresses VEGF-induced angiogenesis, and inhibition of semaphorin3A leads to enhancement of angiogenesis [29]. This phenomenon occurs because semaphorin3A and VEGF share the same receptor, neuropilin1 [30]. In addition, blood vessels are believed to play important roles in tissue repair and axonal regeneration after SCI [31-33]. Therefore, we analyzed the effects of SM-345431 treatment (using our DDS) on angiogenesis. For immunohistochemistry, we used the anti-RECA-1 antibody, which is known to enable visualization of blood vessels and migrating endothelial cells in rats [32] (Figure 4A). RECA-1-positive areas 3 mm caudal to the lesion epicenter were significantly increased after combined treatment (Figure 4C, $P < 0.05$). Based on their morphology, thick-walled blood vessels with lumen diameters larger than 20 μm are thought to be newly formed blood vessels [34] (Figure 4A,B, arrows). Consistent with previous reports [34,35], these thick-walled blood vessels were rarely observed in the intact spinal cord. In comparison to the control group, the total immunostained areas of vessels with lumen diameters larger than 20 μm were significantly increased in both the SM-345431 and combined treatment groups 3 mm rostral/caudal and 1 mm rostral/caudal to the lesion epicenter (Figure 4D). Furthermore, the effects of angiogenesis tended to be enhanced in the combined treatment group compared to the SM-345431 treatment group, but this difference did not reach statistical significance (Figure 4C,D). Thus, SM-345431 treatment significantly increased the number of newly formed blood vessels.

Semaphorin3A also inhibits oligodendrocyte precursor cell recruitment and influences remyelination [36]. Using immunohistochemistry and electron microscopy, we next characterized the axons at the lesion sites after SM-345431 treatment in greater detail. In the SM-345431 treatment group, we observed substantial numbers of myelinated GAP43-positive axons at the lesion site (Figure 4H-J), whereas myelinated GAP43-positive axons were rarely observed at the lesion site in the control SCT group (Figure 4E-G). Based on their morphologies, the thin

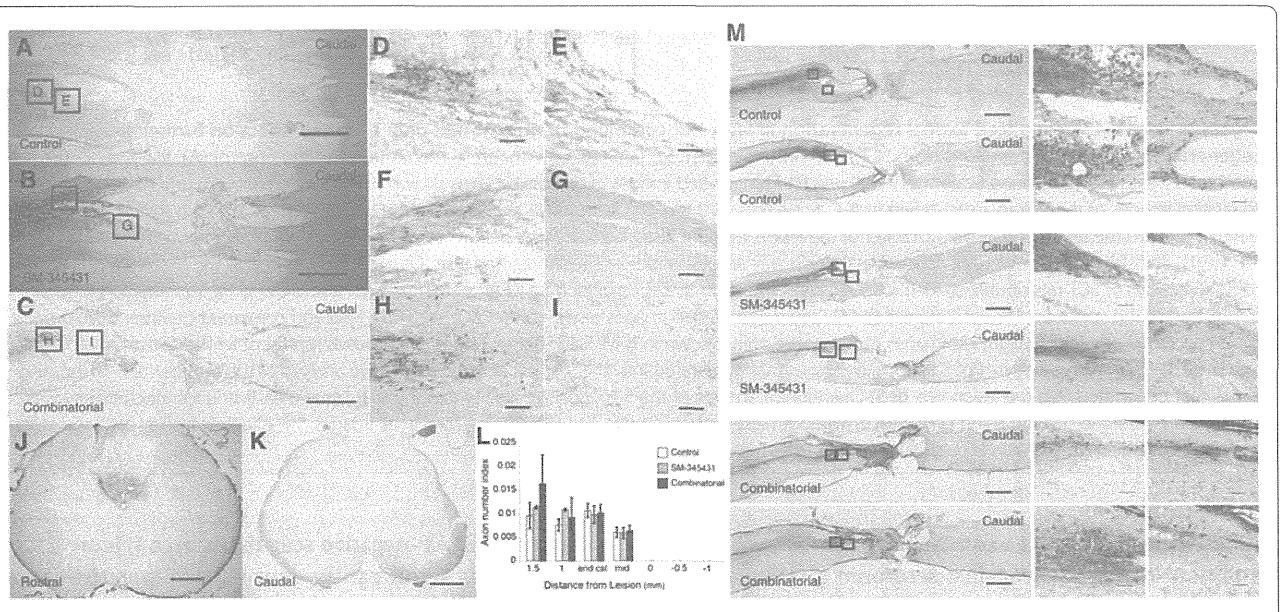

Figure 3 Histological analyses of the treatment effects on CST regeneration in the injured spinal cord using BDA staining. J shows a representative axial section of the spinal cord at the C4 level (rostral to the lesion site), and **K** shows a representative image of a section at the L4 level (caudal to the lesion site) (Scale bars = 500 μm). Based on these sections, we confirmed that the labeling efficiency of BDA tracing in each animal was sufficient. **A**, **B** and **C** show representative sagittal sections of the BDA staining in each group. **D/E** show magnified images of the boxed area in **A**. Similarly, **F/G** show magnifications of the areas in **B**, and the images in **H/I** are magnifications of the areas in **C**. Scale bars = 1,000 μm in **A-C** and 100 μm in **D-I**. No obvious CST regeneration beyond the lesion epicenter was observed in any of the groups examined **(L)**. Statistical analyses were performed using one-way ANOVA and Bonferroni *post hoc* analyses. Data are presented as the mean ± S.E.M. The images in **M** are representative of other sagittal sections from each group. Scale bars = 1,000 μm in the images on left side of **M** and 100 μm in the magnified images of **M**.

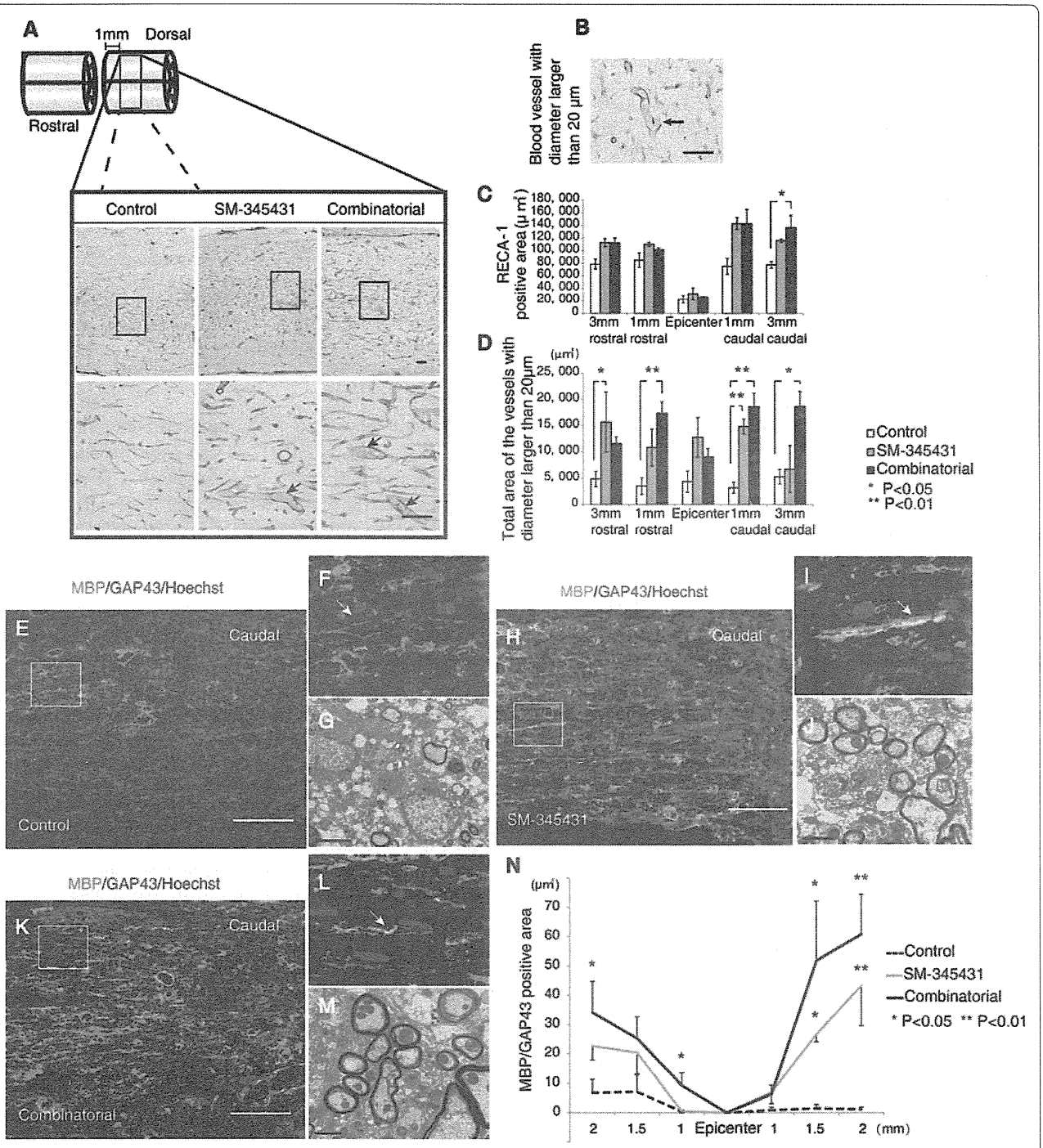

Figure 4 (See legend on next page.)

(See figure on previous page.)
Figure 4 Histological analyses of the treatment effects on microvasculature and remyelination in the spinal cord. (A) Visualization of blood vessels using an anti-RECA-1 antibody. Images in the upper row are low-magnification views of the gray matter areas of sagittal sections immunostained for RECA-1 at 1 mm caudal to the transected site. Scale bars = 50 μm. Images in the lower row are high-magnification views that correspond to the boxed areas in the upper row images. Scale bars = 50 μm. **(B)** Representative image of a blood vessel with a lumen with a diameter larger than 20 μm (arrow), which indicated newly formed blood vessels following injury. Scale bars = 50 μm. Arrows in **(A)** also represent blood vessels with lumen diameters larger than 20 μm. The left side is rostral **(A,B)**. **(C)** Quantitative analysis of RECA-1-positive areas in each group. **(D)** Quantitative analysis of the total areas of RECA-1-positive blood vessels with lumen diameters larger than 20 μm. *$P < 0.05$, **$P < 0.01$. Statistical analyses were based on one-way ANOVA and Bonferroni post hoc analyses. **(E-M)** Analyses of remyelination performed using immunohistochemistry against MBP or electron microscopy 12 weeks post-injury. **(E,F,H,I,K,L)** Reconstructed confocal images showing double staining (sagittal sections) for MBP (green) and GAP43 (red) in the control group **(E,F)**, SM-345431 treatment group **(H,I)** and combined group **(K, L)**. **F**, **I** and **L** show magnified images of the boxed areas in **E**, **H** and **K**, respectively. Scale bars = 100 μm. The arrow in **F** shows a non-myelinated (MBP-negative) GAP-43-positive axon, and the arrows in **I** and **L** show myelinated (MBP-positive) GAP-43-positive axons. The left side is rostral. **(G,J)** Electron microscopic images of transverse sections from the control group **(G)** and SM-345431 treatment group **(J)** at the lesion site. Scale bars = 2 μm. **(N)** Statistical analysis of the number of myelinated (MBP-positive) GAP-43-positive axons in each group, which were analyzed by immunohistochemistry. *$P < 0.05$, **$P < 0.01$. Statistical analyses were performed using one-way ANOVA and Bonferroni *post hoc* analyses. All the data are represented as the mean ± S.E.M.

myelin sheathes observed in the SM-345431 group were likely the result of remyelination (Figure 4H-J). While SM-345431 treatment significantly enhanced the remyelination of axons (Figure 4N), additional remyelination was not observed in the SM-345431 plus treadmill training combined group (Figure 4K-N).

Combining SM-345431 with treadmill training reinforced specific spinal locomotor circuitry and synaptic connectivity

Functional locomotor recovery in spinal cord models is critically dependent on supraspinal connections to CPGs [37]. To examine the combined effects of SM-345431 treatment and treadmill training on the reconstruction of spinal cord circuitry at the lumbar level, we performed immunostaining for c-Fos [38] and synapsin-1 [39,40]. c-Fos is widely used as a marker to measure the extent of the supraspinal drive of specific spinal locomotor circuitries because c-Fos expression in neurons normally increases when after the control of spinal locomotor circuitries' circuitry control is lost [41,42]. Consistent with previous studies, c-Fos expression in nuclei (c-Fos + nuclei) was observed in all rats in levels L1-L5 (Figure 5A-C) [43]. In addition, the number of c-Fos + nuclei tended to be lower at the L1-L5 levels in SM-345431-treated SCI rats than in control SCI rats, but this difference did not reach statistical significance (Figure 5B). Interestingly, the combined treatment group showed a statistically significant decrease in the number of c-Fos + nuclei compared to control SCT rats at the L4 and L5 levels (Figure 5B, $P < 0.01$). We also compared the rostral (L1 + L2) and caudal (L4 + L5) segments of the lumbar enlargement to examine the overall effects of combinatorial treatment (Figure 5C). Compared to the intact group (normal rats), control SCT rats showed a significant increase in c-Fos + nuclei counts in the caudal segments of the lumbar enlargement (L4-5), which is consistent with previous reports (Figure 5C, $P < 0.01$) [24]. On the other hand, after combined treatment, the caudal segments of the lumbar enlargement showed significantly decreased c-Fos + nuclei counts (Figure 5C, $P < 0.01$) as compared to control SCT rats. The number of c-Fos + nuclei also tended to be decreased after SM-345431 treatment alone, although this difference was not statistically significant (Figure 5C). Thus, specific spinal locomotor circuitries, especially in the caudal sections of the lumbar enlargement, were considerably reinforced by combined treatment and, to a lesser extent, by SM-345431 treatment alone.

Synapsin-1, a widely used presynaptic marker, has been used to examine activity-dependent synaptic plasticity and synaptic function [39,40]. In comparison to the control and SM-345431 groups, a statistically significant increase in synapsin-1 expression was observed at the lumbar enlargement level (Figure 5E-N) ($P < 0.01$ compared to the control SCT group; $P < 0.05$ compared to the SM-345431 group) in the combined treatment group. No statistically significant difference was observed between the SM-345431 group and the control SCT group ($P > 0.05$). These results indicated that, while SM-345431 treatment alone had a limited effect, SM-345431 treatment combined with treadmill training significantly reinforced synaptic plasticity and function at the lumbar enlargement level.

Taken together, these data suggest that reinforcement of specific spinal locomotor circuitries and motor learning occurred in the lumbosacral circuits of adult rats after combined treatment. These effects were also observed, to a lesser extent, after SM-345431 treatment alone.

SM-345431 promoted motor functional recovery and combined treatment enhanced this recovery

Next, we investigated the hindlimb motor functions of rats while they walked on a treadmill (induced by a robotic device) using kinematic analysis. In the control SCT rats, hindlimb motor functions showed almost no recovery throughout the period of our experiments (3 months). The SCT rats were unable to take any steps on a treadmill even 3 months post-injury, whereas the treated animals

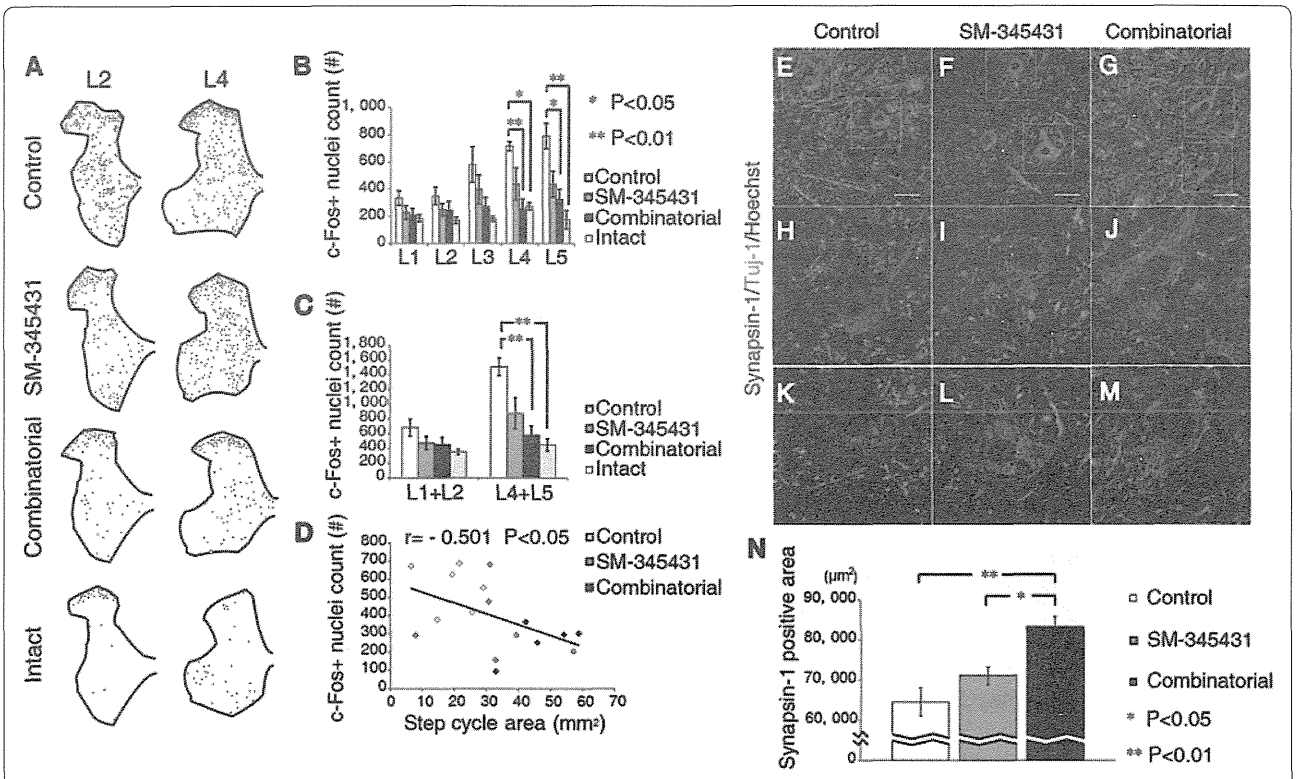

Figure 5 Immunohistochemical analyses of the effects of treatment on functional remodeling of spinal circuits and synaptic connectivity at the lumbar enlargement. (A) Representative Camera Lucida drawings of c-Fos + nuclei in transverse sections at the L2 and L4 levels from control rats, SM-345431 treatment rats, combined treatment rats and intact rats. **(B)** Average total numbers of c-Fos + nuclei at each level of the lumbar spinal segment. **(C)** Average total number of c-Fos + nuclei in rostral (L1 + L2) and caudal (L4 + L5) lumbar enlargement segments. **(D)** Correlation analysis between the total number of c-Fos + nuclei in all segments of the lumbar enlargement and step ability on the treadmill. SM-345431 treatment produced a trend toward decreases in the average number of c-Fos + nuclei, although this trend was not statistically significant compared to the control and SM-345431 treatment groups. However, the combined treatment produced a statistically significant decrease in the number of c-Fos + nuclei, suggesting that specific spinal locomotor circuitry was reinforced by combining SM-345431 treatment with extensive treadmill training. *P < 0.05, **P < 0.01. Statistical analyses were performed using one-way ANOVA and Bonferroni post hoc analyses. Data are presented as the mean ± S.E.M. **(E-M)** Representative reconstructed confocal images of double staining (transverse section) for synapsin-1 and Tuj-1 in the ventricolumnar area of the spinal cord (**E-G**: low-magnification images, **H-M**: high-magnification images). **H-J** and **K-M** show the upper and lower boxed areas in **E-G**, respectively. Scale bars = 50 μm. **(N)** Quantitative analysis of synapsin-1 expression in the ventricolumnar motor neuron area 3 months after SCT. *P < 0.05, **P < 0.01. Statistical analyses were performed using one-way ANOVA and Bonferroni *post hoc* analyses. Data are presented as the mean ± S.E.M.

showed some degree of motor function recovery. We performed Bonferroni *post hoc* analyses to examine the differences in step length and step height between the groups (Figure 6A) and found that motor function was significantly better in SM-345431 rats than in control SCT rats (Figure 6B-C). Furthermore, SM-345431 treatment with treadmill training further improved motor performance as compared to no treatment (Figure 6B,C,D,E) or SM-345431 treatment alone (Figure 6D,E). To evaluate motor functions in greater detail, we examined the "step cycle area", which was calculated by multiplying the average step length and average step height as previously described [44] (Figure 6F). This parameter includes elements of both the horizontal and vertical step planes and can thus be regarded as a 2-dimensional evaluation of each step taken. We again performed Bonferroni *post hoc* analyses to statistically compare the differences between the groups. In the SM-345431-treated rats, a statistically significant enhancement of the step cycle area was observed in comparison to the control SCT rats ($P < 0.05$ at 3 months). Furthermore, the combined treatment resulted in an even greater improvement in step cycle area when compared to control SCT rats ($P < 0.05$ at the first month, $P < 0.01$ at the second month, $P < 0.01$ at the third month). As previously described [20], the control SCT rats could not take any steps on the treadmill even at 3 months post-injury (Figure 6G,H and Additional file 1). Without extensive treadmill training, the effects of SM-345431 treatment were moderate and did not result in plantar step walking, even with the BSS (Figure 6G,H and Additional file 1). However, when combined with extensive treadmill training, SM-345431 treatment led

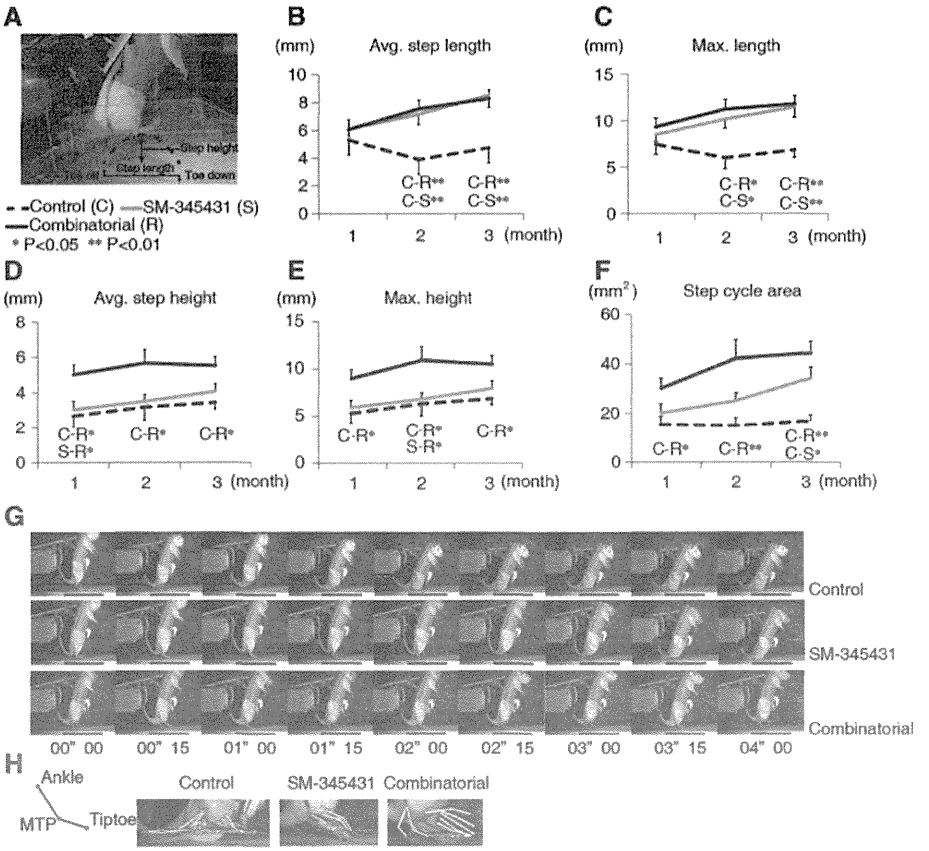

Figure 6 Detailed kinematic analysis of hindlimb motor performance on the treadmill. (A) Representative image of the analysis and a schematic diagram of the step parameters. Collected kinematic data from each group showing the average step lengths **(B)**, maximum step lengths **(C)**, average step heights **(D)**, maximum step heights **(E)** and step cycle areas **(F)**. All of these data were recorded and analyzed using a robotic device (Rodent Robot 3000; Robomedica Inc.). Each kinematic analysis was performed at 70% BWS and a speed of 1 cm/s over 1 min. C represents the control group, S represents the SM-345431 group, and R represents the combined treatment group. *P < 0.05, **P < 0.01. C-S* indicates that a statistically significant difference was observed between the control and SM-345431 groups at P < 0.05. Statistical analyses were performed using one-way ANOVA with Bonferroni *post hoc* analyses. Data are presented as the means ± S.E.M. **(G)** Representative sequential pictures of steps taken during the first 4 s of the analysis (BWS: 70%, speed: 3 cm/s). **(H)** Kinematic characteristics of the first step taken in each group. SM-345431 treatment enhanced motor function recovery on the treadmill, especially in terms of the step length parameters. Combined treatment further enhanced the motor function recovery, especially in terms of the step height and step cycle area parameters.

to considerably enhanced motor function recovery; all rats exposed to the combined treatment achieved continuous plantar step walking on a treadmill with the BSS for at least 30 min (Figure 6G,H and Additional file 1).

Specifically, SM-345431 treatment improved locomotor function on a treadmill after SCT particularly in terms of the step length parameters (Figure 6B,C: average and maximum step lengths). Regarding the step height parameter, the effect of SM-345431 treatment was moderate and statistically insignificant (Figure 6D,E). However, when SM-345431 treatment was combined with extensive treadmill training, greater enhancement was observed, and this enhancement extended to the step height parameter (Figure 6D,E; average and maximum step heights). Furthermore, the incremental effects of the treatments over time on motor function performance, specifically on step height and step cycle area, did not reach a plateau by the end of the experimental period (3 months post-injury). At this time, the incremental effects tended to be more robust in the SM-345431 treatment group than in the combined treatment group (Figure 6F: step cycle area). Interestingly, we also discovered a statistically significant correlation between the number of c-Fos + nuclei and motor function (step cycle area) within each group; the c-Fos + nuclei counts were inversely correlated with the extent of functional motor recovery (Figure 5D; r = -0.501, P < 0.05).

We next examined the extent to which the regenerated axons at the lesion sites contributed to motor function recovery in each group. We performed re-transection of the initial lesion site 12 weeks after the initial injury, and we also performed the kinematic analysis before and after the re-transectioning procedure. None of the step parameters changed significantly in the control group, whereas the

step cycle area tended to be attenuated in the SM-345431 group after re-transection (Figure 7). Interestingly, greater attenuations of step ability were observed in all analyzed parameters in the combined treatment group after re-transection, and some of these parameters (step height) were statistically significant (Figure 7, average step height: $P < 0.01$; maximum step height: $P < 0.05$). Thus, the regenerated axons at the lesion site contributed, at least partially, to the enhancement of motor function recovery.

Discussion

With clinical applications in mind, we first sought to find an appropriate and efficient way to deliver our semaphorin3A inhibitor to transected spinal cords to reestablish useful motor function after SCI. For this purpose, we developed a novel DDS and tested its therapeutic potential *in vivo*. Furthermore, we tested whether specific rehabilitation had the capability to reinforce motor function in the SCT model after treatment with the semaphorin3A inhibitor. Our results can be briefly summarized as follows. First, our newly developed DDS utilizing silicone sheets provided continuous and stable drug delivery and therefore demonstrated potential clinical application. Second, motor function recovery was considerably enhanced by combining SM-345431, the novel semaphorin3A inhibitor, with treadmill training, and this combined treatment enabled paralyzed rats to perform continuous plantar step walking on a treadmill with a BSS.

Osmotic mini pumps have been widely used for drug delivery in animal models of SCI [20,45]. While these pumps are excellent for controlling the drug release dosage and the accurate positioning of drug delivery, this method is too invasive for use in most patients. Therefore, we developed a new silicone matrix preparation as a novel DDS and showed that this novel DDS provided stable and continuous release of SM-345431 throughout the experimental period. In addition, because SM-345431 shows a better stability in a silicone sheet than SM-216289 and approximately the same semaphorin3A inhibitory activity as SM-216289, we used SM-345431 instead of SM-216289 in the present study. As a result, significantly enhanced axonal regeneration and motor function recovery were observed after SM-345431 treatment, which is consistent with our previous study using SM-216289 and osmotic mini pumps [20]. Therefore, this novel DDS demonstrated strong potential for future clinical use.

In this study, we examined the effects of a new semaphorin3A inhibitor, SM-345431, on axonal regeneration and motor function recovery after SCT. Our data indicated that SM-345431 administration using the novel DDS was effective in promoting axonal regeneration and motor function recovery *in vivo*. However, consistent with the results of our previous study using SM-216289, these effects were moderate [20]. More importantly, we found that motor function recovery was significantly enhanced by combining SM-345431 with extensive treadmill training (Figure 6). This combined strategy enabled paralyzed rats to perform continuous plantar step walking on a treadmill with a BSS. Previous work has also demonstrated that intact or injured axons in descending tracts and propriospinal circuits can undergo spontaneous anatomical and physiological remodeling after SCI [46,47] to allow the relay of information through endogenous spinal circuits. Subsequently, the novel propriospinal relay connections bypass the injury epicenter to induce supraspinal control and some degree of motor function recovery. This phenomenon has also been observed following the irreversible interruption of long descending tracts in mice [48]. Because SM-345431 treatment without extensive treadmill training had limited effects on anatomical reconstruction in the lumbar enlargement

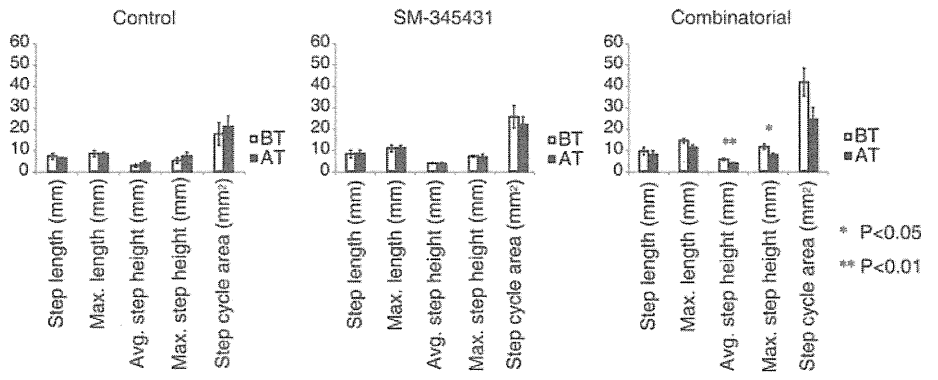

Figure 7 Detailed kinematic analyses of hindlimb motor performance on a treadmill before and after re-transection. Detailed kinematic analyses of hindlimb motor performance on a treadmill before and after re-transection were performed and analyzed using a robotic device (Rodent Robot 3000; Robomedica Inc.). BT represents before re-transection; AT represents after re-transection. Although none of the step parameters in the control group showed significant changes, the step cycle area parameters were attenuated in the SM-345431 group after re-transection. Further attenuation of the step ability parameters was observed in the combined treatment group after re-transection. *$P < 0.05$ **$P < 0.01$. Statistical analyses were performed using *t*-test analyses. Data are presented as the mean ± S.E.M.

(Figure 5), we speculate that the enhanced motor function recovery observed after SM-345431 treatment resulted mainly from axon regeneration and limited anatomical reconstruction. Enhanced axonal regeneration possibly led to anatomical and physiological remodeling at the lesion site and improved motor function recovery, which is consistent with our previous findings using SM-216289 administered via osmotic mini pumps [20].

Interestingly, while axonal regeneration was not further enhanced by combining SM-345431 treatment with extensive treadmill training (Figure 2), motor function recovery was significantly enhanced (Figure 6). Previous work demonstrated that limited spontaneous axonal regeneration occurs after SCI and that only some of the new axons are useful for motor function recovery [49]. Thus, axonal regeneration alone may not result in sufficient motor function recovery unless these regenerated axons are appropriately connected. We therefore hypothesized that the regenerated axons induced by semaphorin3A inhibitor treatment may exhibit substantially improved rewiring, in terms of the formation of appropriate connections, following extensive treadmill training. Indeed, motor function recovery was enhanced significantly by combined treatment, as paralyzed rats that received combined treatment were able to perform continuous plantar step walking on a treadmill with a BSS (Figure 6). Re-transectioning experiments further suggested that the regenerated axons at the lesion site and their rewiring contributed to the enhancement in motor function recovery observed in the treatment groups (Figure 7). We also observed that some regenerated axons, such as 5-HT-positive raphespinal tract axons, penetrated into the epicenter of the lesion (Figure 2), and these regenerated axons may have contributed to the reorganization of spinal circuitry at the lesion site and enhanced motor function recovery in the treatment groups [20]. Interestingly, we observed greater attenuation of motor function after re-transection in the combined treatment group (Figure 7). Taken together, these data indicate that the regenerated axons achieved substantial rewiring to the appropriate targets at the lesion site, which was associated with the rehabilitation performed in the combined treatment group [21].

Moreover, the enhanced motor function recovery was only partially attenuated after re-transection in the treatment groups. The results of these re-transection experiments in the treatment groups, especially in the combined treatment group, suggested that other factors, such as reorganization of the lumbar spinal circuitry, also contributed to the enhancement of motor function recovery. We also performed re-transection experiments in animals that only received extensive treadmill training (without SM-345431 treatment), and in these animals, only minimum attenuation of motor performance after re-transection was observed (data not shown). This finding further supports the mechanism proposed above. Taken together, it is possible that specific rehabilitation enhances not only the rewiring of the regenerated axons but also the reorganization of the lumbar spinal circuitry [43]. Furthermore, in the combined treatment group, it is possible that the effect of specific rehabilitation on the reorganization of the lumbar spinal circuitry was the main contributor to the enhancement of motor function recovery in the early stage, while the effect on rewiring of the regenerated axons was the main contributor to the enhancement of motor function recovery during the later stage.

The results of c-Fos immunohistochemistry (Figure 5) showed that extensive treadmill training induced plastic changes at a level caudal to the injured site. Interestingly, step ability on the treadmill was significantly correlated with decreases in the numbers of c-Fos-positive nuclei at a level caudal to the lumbar enlargement (Figure 5D). Therefore, enhanced motor function recovery could be partially the result of anatomical reconstruction of the lumbar spinal cord, which is thought to be the location of CPGs [50]. It is now widely accepted that supraspinal drive of CPGs is required for locomotor function [51] and that the intrinsic plasticity of CPGs allows some spontaneous motor function recovery even in the absence of significant axonal regeneration [24,52]. Therefore, it is possible that axon regeneration moderately enhanced motor function recovery in the SM-345431 treatment group, while rewiring of the regenerated axons and CPG activation was achieved by combining the SM-345431 treatment with treadmill training.

Which segment of the lumbar enlargement is most important for improved walking ability on a treadmill? Reportedly, rhythmic bursts are related to flexor activity at the L2 level and to extensor activity at the L5 level [50]. Treadmill training induces plastic changes in the transmission of group I pathways to extensors that consequently support the recovery of weight-supported motion while standing [53]. The present study showed that combined treatment significantly altered c-Fos expression at the L4 and L5 levels (Figure 5B-C) and improved step height (Figure 6D-E) and continuous plantar step walking on the treadmill with a BSS (Figure 6G and Additional file 1). However, while SM-345431 alone improved step ability, this improvement did not lead to continuous plantar step walking (Figure 6). Therefore, axon regeneration alone might have only limited effects on the spinal cord extensor pool, which could explain the limited motor function recovery of SCT rats after SM-345431 treatment alone. However, the combined treatment may have reestablished the function of the extensor pool by rewiring the regenerated axons and remodeling spinal circuits. As a result, important motor functions, such as continuous plantar step walking (on a treadmill with a BSS), may have been reestablished in SCT adult rats in the combined